

4.0 CRITICALITY SAFETY EVALUATION

4.1 Design Bases

This report documents the criticality safety evaluation for the storage of PWR spent nuclear fuel in Holtec Region 1 & 2 style high-density spent fuel storage racks at the V.C. Summer nuclear power plant operated by South Carolina Electric & Gas (SCE&G). The objective of this analysis is to ensure that the effective neutron multiplication factor (k_{eff}) is less than or equal to 0.95 with the storage racks fully loaded with fuel of the highest anticipated reactivity and the pool flooded with unborated water at a temperature corresponding to the highest reactivity. The maximum calculated reactivity includes a margin for uncertainty in reactivity calculations including manufacturing tolerances and is shown to be less than 0.95 with a 95% probability at a 95% confidence level [4.1.1]. Reactivity effects of abnormal and accident conditions have also been evaluated to assure that under all credible abnormal and accident conditions, the reactivity will not exceed the regulatory limit of 0.95.

Applicable codes, standards, and regulations or pertinent sections thereof, include the following:

- *Code of Federal Regulations*, Title 10, Part 50, Appendix A, General Design Criterion 62, "Prevention of Criticality in Fuel Storage and Handling."
- USNRC Standard Review Plan, NUREG-0800, Section 9.1.2, Spent Fuel Storage, Rev. 3 - July 1981.
- USNRC letter of April 14, 1978, to all Power Reactor Licensees - OT Position for Review and Acceptance of Spent Fuel Storage and Handling Applications, including modification letter dated January 18, 1979.
- L. Kopp, "Guidance on the Regulatory Requirements for Criticality Analysis of Fuel Storage at Light-Water Reactor Power Plants," NRC Memorandum from L. Kopp to T. Collins, August 19, 1998.
- USNRC Regulatory Guide 1.13, Spent Fuel Storage Facility Design Basis, Rev. 2 (proposed), December 1981.

- ANSI ANS-8.17-1984, Criticality Safety Criteria for the Handling, Storage and Transportation of LWR Fuel Outside Reactors.

USNRC guidelines [4.1.2] and the applicable ANSI standards specify that the maximum effective multiplication factor, k_{eff} , including bias, uncertainties, and calculational statistics, shall be less than or equal to 0.95, with 95% probability at the 95% confidence level.

To assure the true reactivity will always be less than the calculated reactivity, the following conservative design criteria and assumptions were employed:

- Moderator is unborated water at a temperature that results in the highest reactivity (4°C, corresponding to the maximum possible moderator density, 1.000 g/cc).
- The racks were assumed to be fully loaded with the most reactive fuel authorized to be stored in the racks.
- No soluble poison (boron) is assumed to be present in the pool water under normal operating conditions, except for the fuel assembly in-transit condition.
- Neutron absorption in minor structural members is neglected, i.e., spacer grids are replaced by water.
- The effective multiplication factor of an infinite radial array of fuel assemblies was used in the analyses, except for the assessment of peripheral effects and certain abnormal/accident conditions where neutron leakage is inherent.
- In-core depletion calculations assume conservative operating conditions, highest fuel and moderator temperature, and an allowance for the soluble boron concentrations during in-core operations.
- For assemblies that use WABAs during in-core depletion, it is assumed that the maximum burnup of the assembly when the WABA is removed is 30 GWD/MTU.

The spent fuel storage racks are designed to accommodate the fuel assembly types listed in Table 4.1.1 with a maximum nominal initial enrichment of 4.95 wt% ^{235}U .

Two separate storage regions are provided in the V.C. Summer spent fuel pools. The independent acceptance criteria for storage in each of the regions are as follows:

- ⇒ Region 1 is designed to accommodate fresh or burned fuel assemblies with a maximum nominal initial enrichment of 4.95 wt% ^{235}U .
- ⇒ Region 2 is designed to accommodate fuel assemblies with a maximum nominal initial enrichment of 4.95 wt% ^{235}U which have accumulated a minimum burnup of 41.6 GWD/MTU or fuel of initial enrichment and burnup combinations within the acceptable domain depicted in Figure 4.1.1.

The water in the spent fuel storage pool normally contains soluble boron, which would result in a large sub-criticality margin under actual operating conditions. However, the NRC guidelines, based upon the accident condition in which all soluble poison is assumed to have been lost, specify that the limiting k_{eff} of 0.95 for normal storage be evaluated for the accident condition that assumes the loss of soluble boron. The double contingency principle of ANSI N-16.1-1975 and of the April 1978 NRC letter allows credit for soluble boron under other abnormal or accident conditions, since only a single independent accident need be considered at one time. Consequences of abnormal and accident conditions have been evaluated, where "abnormal" refers to conditions which may reasonably be expected to occur during the lifetime of the plant and "accident" refers to conditions which are not expected to occur but nevertheless must be protected against.

4.2 Summary of Criticality Analyses

4.2.1 Normal Operating Conditions

The criticality analyses for each of the two separate regions of the spent fuel storage pool are summarized in Tables 4.2.1 and 4.2.2, for the design basis storage conditions. For the fuel acceptance criteria defined in the previous section, the maximum k_{eff} values are shown to be less than 0.95 (95% probability at the 95% confidence level) in each of the regions.

4.2.1.1 Region 1

Calculations have been performed to qualify the Region 1 racks for storage of fresh unburned fuel assemblies with a maximum nominal initial enrichment of 4.95 wt% ²³⁵U. The criticality analyses for Region 1 of the spent fuel storage pool are summarized in Table 4.2.1, and demonstrate that for the defined acceptance criteria, the maximum k_{eff} is less than 0.95.

4.2.1.2 Region 2

Calculations have been performed to qualify the Region 2 racks for storage of spent fuel assemblies with a maximum nominal initial enrichment of 4.95 wt% ²³⁵U which have accumulated a minimum burnup of 41.6 GWD/MTU or fuel of initial enrichment and burnup combinations within the acceptable domain depicted in Figure 4.1.1. The criticality analyses for Region 2 of the spent fuel storage pool are summarized in Table 4.2.2, and demonstrate that for the defined acceptance criteria, the maximum k_{eff} is less than 0.95.

The calculated maximum reactivity in Region 2 includes the reactivity effect of the axial distribution in burnup and provides an additional margin of uncertainty for the depletion calculations. The data points shown in Figure 4.1.1 are tabulated in Table 4.2.3. For convenience, the minimum (limiting) burnup data may be described as a function of the nominal initial enrichment, E , in wt% ²³⁵U by a bounding polynomial expression as follows:

$$B = 0.1246 \times E^3 - 1.9100 \times E^2 + 20.9205 \times E - 30.2582,$$

where B is the minimum burnup in GWD/MTU and E is the enrichment in wt% ²³⁵U (for initial enrichments from 2.0 to 4.95 wt% ²³⁵U). Fuel assemblies with enrichments less than 2.0 wt% ²³⁵U will conservatively be required to meet the burnup requirements of 2.0 wt% ²³⁵U assemblies as shown in Fig 4.1.1. Alternatively, since the data are nearly linear, linear interpolation between the points listed in Table 4.2.3 is acceptable.

The criteria identified above for acceptable storage in each of the regions will be implemented by Technical Specifications.

4.2.2 Abnormal and Accident Conditions

Although credit for the soluble poison normally present in the spent fuel pool water is permitted under abnormal or accident conditions, most abnormal or accident conditions will not result in exceeding the limiting reactivity even in the absence of soluble poison. The effects on reactivity of credible abnormal and accident conditions are discussed in Section 4.7 and summarized in Table 4.2.4. Strict administrative procedures to assure the presence of soluble poison will preclude the possibility of the simultaneous occurrence of the two independent accident conditions.

The abnormal location of a fresh fuel assembly has the potential for exceeding the limiting reactivity, should there be a concurrent and independent accident condition resulting in the loss of all soluble poison. Assuring the presence of soluble poison during fuel handling operations will preclude the possibility of the simultaneous occurrence of the two independent accident conditions. The largest reactivity increase would occur if a fresh fuel assembly of the highest permissible enrichment (4.95 wt% ^{235}U) were to be inadvertently loaded into a Region 2 storage cell with the remainder of the rack fully loaded with fuel of the highest permissible reactivity. Under this accident condition, credit for the presence of soluble poison is permitted by the NRC guidelines¹. Calculations indicate that a minimum soluble boron concentration of 400 ppm is more than adequate to assure that keff remains below 0.95.

Additionally, the misplacement of a fresh fuel assembly outside and adjacent to the Region 2 racks during rack installation has the potential for exceeding the limiting reactivity, should there be a concurrent and independent accident condition resulting in the loss of all soluble boron. Assuring the presence of soluble boron during the rack installation procedure will preclude the possibility of the simultaneous occurrence of two independent accident conditions. The largest reactivity increase would

¹ Double contingency principle of ANSI N16.1-1975, as specified in the April 14, 1978 NRC letter (Section 1.2) and implied in the proposed revision to Reg. Guide 1.13 (Section 1.4, Appendix A).

occur if a fresh fuel assembly of the highest permissible enrichment (4.95 wt% ^{235}U) were to be inadvertently misplaced outside and adjacent to a Region 2 storage cell with the remainder of the rack fully loaded with fuel of the highest permissible reactivity and no Boral panel between the fuel in the storage rack and the misplaced assembly. Calculations indicate that a minimum soluble boron concentration of 425 ppm is more than adequate to assure that k_{eff} remains below 0.95.

4.3 Reference Fuel Storage Cells

4.3.1 Reference Fuel Assembly

The spent fuel storage racks are designed to accommodate Westinghouse 17x17 Standard, Westinghouse 17x17 Vantage 5, and Westinghouse 17x17 Performance fuel assemblies. The design specifications for these fuel assemblies, which were used for this analysis, are given in Table 4.1.1. In terms of dimensions that are important to reactivity, the Westinghouse 17x17 Vantage 5 and Westinghouse 17x17 Performance fuel assembly types listed in Table 4.1.1 are identical; herein either of these two assemblies will be referred to as the Westinghouse 17x17 Vantage assembly. Calculations to determine the most reactive assembly type in both the Region 1 and Region 2 storage racks were performed. For the Region 1 rack the reference fuel assembly was determined to be the Westinghouse 17x17 Standard assembly. For the Region 2 racks, the reference fuel assembly was determined to be the Westinghouse 17x17 Standard assembly under normal conditions for the entire range of the burnup versus enrichment curve identified in Figure 4.1.1. For accident conditions, where a fresh unburned assembly is assumed to be placed in or adjacent to the Region 2 rack surrounded by fuel with the appropriate burnup for its manufactured initial enrichment, the Westinghouse 17x17 Vantage has the highest reactivity and is therefore considered the reference assembly.

4.3.2 Region 1 Fuel Storage Cells

Figure 4.3.1 shows the calculational model of the nominal Region 1 spent fuel storage cell containing the Westinghouse 17x17 fuel assembly. The Region 1 storage cells are composed of stainless steel boxes separated by a gap with fixed neutron absorber panels, Boral, centered on each side in a 1/4 inch

channel. The thick steel walls define the storage cells, which have a inch nominal inside dimension. A inch stainless steel sheath supports the Boral panel and defines the boundary of the flux-trap water-gap used to augment reactivity control. The cells are located on a lattice spacing of inches in both directions. Stainless steel channels connect the storage cells in a rigid structure and define the flux-trap of inches, between the sheathing of the Boral panels. The Boral absorber has a thickness of inches and a nominal B-10 areal density of . The Boral absorber panels are inches in width and inches in length. Boral panels are installed on all exterior walls facing other racks, but are not placed on exterior walls that face non-fueled regions. The minimum gap between neighboring Region 1 style racks and between Region 1 and Region 2 style racks is greater than 2.0 inches.

4.3.3 Region 2 Fuel Storage Cells

Figure 4.3.2 shows the calculational model of the nominal Region 2 spent fuel storage cell containing the Westinghouse 17x17 fuel assembly. The Region 2 storage cells are composed of stainless steel walls with a single fixed neutron absorber panel, Boral, (attached by a stainless steel sheathing) centered on each side in a inch channel. Stainless steel boxes are arranged in an alternating pattern such that the connection of the box corners form storage cells between those of the stainless steel boxes. These cells are located on a lattice spacing of inch. The thick steel walls define a storage cell, which has a inch nominal inside dimension. The Boral absorber has a thickness of inch and a nominal B-10 areal density of . The Boral absorber panels are inches in width and inches in length. Boral panels are installed on one side of neighboring Region 2 racks. Boral panels are not installed on exterior walls facing non-fueled regions, i.e., the pool walls. The minimum gap between neighboring Region 2 style racks is 1.0 inch, while the minimum gap between Region 1 and Region 2 style racks is greater than 2.0 inches.

4.4 Analytical Methodology

4.4.1 Reference Design Calculations

The principal methods for the criticality analyses of the high density storage racks include the following codes: (1) MCNP4a [4.4.1], (2) KENO5a [4.4.2], and (3) CASMO-4 [4.4.5-4.4.7]. MCNP4a is a continuous energy three-dimensional Monte Carlo code developed at the Los Alamos National Laboratory. KENO5a is a three-dimensional multigroup Monte Carlo code developed at the Oak Ridge National Laboratory as part of the SCALE 4.3 package [4.4.3]. The KENO5a calculations used the 238-group SCALE cross-section library and NITAWL [4.4.4] for ^{238}U resonance shielding effects (Nordheim integral treatment). Benchmark calculations, presented in Appendix 4A, indicate a bias of 0.0009 with an uncertainty of ± 0.0011 for MCNP4a and 0.0030 ± 0.0012 for KENO5a, both evaluated with the 95% probability at the 95% confidence level [4.1.1].

Fuel depletion analyses during core operation were performed with CASMO-4, a two-dimensional multigroup transport theory code based on capture probabilities [4.4.5 - 4.4.7]. Restarting the CASMO-4 calculations in the storage rack geometry yields the two-dimensional infinite multiplication factor (k_{∞}) for the storage rack. Parallel calculations with CASMO-4 for the storage rack at various enrichments enable a reactivity equivalent enrichment (fresh fuel) to be determined that provides the same reactivity in the rack as the depleted fuel. CASMO-4 was also used to determine the reactivity uncertainties (differential calculations) of manufacturing tolerances and the reactivity effects of variations in the water temperature and density.

In the geometric models used for the calculations, each fuel rod and its cladding were described explicitly and reflecting boundary conditions were used in the radial direction, which has the effect of creating an infinite radial array of storage cells. Monte Carlo calculations inherently include a statistical uncertainty due to the random nature of neutron tracking. To minimize the statistical uncertainty of the MCNP4a and KENO5a calculated reactivities and to assure convergence, a minimum of 1 million neutron histories were accumulated in each calculation.

4.4.2 Fuel Burnup Calculations and Uncertainties

CASMO-4 was used for burnup calculations in the hot operating condition. To the extent possible, CASMO-4 has been benchmarked [4.4.6, 4.4.7] against cold, clean, critical experiments (including plutonium-bearing fuel) and Monte Carlo calculations.

In the CASMO-4 geometric models, each fuel rod and its cladding were described explicitly and reflective boundary conditions were used between storage cells. These boundary conditions have the effect of creating an infinite array of storage cells.

Conservative assumptions of moderator and fuel temperatures and the average operating soluble boron concentrations were used to assure the highest plutonium production and hence conservatively high values of reactivity as a function of burnup. Since critical experiment data with spent fuel is not available for determining the uncertainty in depletion calculations, an allowance for uncertainty in reactivity² was assigned based upon other considerations [4.1.2]. Assuming the uncertainty in depletion calculations is less than 5% of the total reactivity decrement, a burnup dependent uncertainty in reactivity for burnup calculations was assigned. Thus, the burnup uncertainty varies (increases) with burnup. This allowance for burnup uncertainty was included in determination of the acceptable burnup versus enrichment combinations.

4.4.3 Effect of Axial Burnup Distribution

Initially, fuel loaded into the reactor will burn with a slightly skewed cosine power distribution. As burnup progresses, the burnup distribution will tend to flatten, becoming more highly burned in the central regions than in the upper and lower regions. At high burnup, the more reactive fuel near the ends of the fuel assembly (less than average burnup) occurs in regions of high neutron leakage. Consequently, it is

²The majority of the uncertainty in depletion calculations derives from uncertainties in fuel and moderator temperatures and the effect of reactivity control methods (e.g., soluble boron). For depletion calculations, bounding values of these operating parameters were assumed to assure conservative results in the analyses.

expected that over most of the burnup history, fuel assemblies with distributed burnups will exhibit a slightly lower reactivity than that calculated for the uniform average burnup. As burnup progresses, the distribution, to some extent, tends to be self-regulating as controlled by the axial power distribution, precluding the existence of large regions of significantly reduced burnup.

Among others, Turner [4.4.8] has provided generic analytic results of the axial burnup effect based upon calculated and measured axial burnup distributions. These analyses confirm the minor and generally negative reactivity effect of the axially distributed burnups at values less than about 30 GWD/MTU with small positive reactivity effects at higher burnup values. For the present criticality analyses, the reference calculations utilized axial burnup distributions from both Holtec International and actual V.C. Summer plant data. Burnup-equivalent enrichments were determined with CASMO-4 for each of axial zones and used in three-dimensional Monte Carlo calculations. Results of these calculations, therefore, inherently include the effect of the axial distribution in burnup. Comparison of these results to results of calculations with uniform axial burnup allows the reactivity effect of the axial burnup distribution to be quantified. This reactivity effect is included, where applicable, in the calculation of the maximum k_{eff} values.

4.4.4 BPRAs

In the first two cycles of operation at the V.C. Summer plant, Burnable Poison Rod Assemblies (BPRAs) were used. These inserts were placed inside the guide tubes of a fresh fuel assembly and removed at the end of the first cycle. The assembly was allowed to burn further in the reactor core for another cycle or two. The assemblies in these two cycles that used BPRAs fall into one of the three groups in Table 4.4.1, based on initial nominal enrichment, cycle burnup and final assembly burnup. For each of these groups the maximum k_{eff} was calculated and shown to be less than the maximum calculated k_{eff} of 0.9485 shown in Table 4.2.1. Therefore all assemblies that used BPRAs in the first two cycles of operation at the V.C. Summer plant are acceptable to stored in the Region 2 fuel storage racks.

4.4.5 Effect of WABA Usage

Wet Annular Burnable Absorber (WABA) rods are fuel assembly inserts placed in the guide tubes of a fresh fuel assembly, which are removed after in-core operation. The fuel assembly is then allowed to burn further in the reactor core. Assemblies that use WABAs have a higher k_{eff} in the spent fuel storage rack than assemblies that do not use WABAs. The difference in reactivity between an assembly that uses a WABA and an assembly that does not use a WABA is determined and applied as a penalty to the burnup versus enrichment curve. The maximum penalty associated with the use of WABAs was based on the maximum number of rodlets, 24, and a maximum fuel assembly burnup of 30 GWD/MTU when the WABA is removed from the assembly.

4.4.6 IFBA Rods

IFBA rods are present in both the Westinghouse 17x17 Vantage 5 and Performance assemblies, but not in the Westinghouse 17x17 Standard assemblies at the V.C. Summer plant. Calculations are performed with assemblies containing up to 156 IFBA rods having a maximum ^{10}B loading of 3.0 mg/inch. The results of these calculations show that a Vantage assembly with IFBA rods has a higher reactivity than a Vantage assembly without IFBA rods, but that the reactivity of the Standard assembly, which is identified as the reference assembly for the Region 2 fuel storage racks in Section 4.3.1, still bounds the reactivity of the Vantage assembly, either with or without IFBA rods. Therefore it is not necessary to apply an additional penalty to the burnup versus enrichment curve to account for the presence of IFBA rods in the Vantage assemblies.

4.4.7 Erbia Rods

Recently, PWR fuel assembly manufacturers have been incorporating Erbium (Er_2O_3) into PWR fuel assemblies, much like Gadolinia is incorporated into the fuel in BWR assemblies, to augment reactivity control during in-core operations. To retain the option of using Erbium rods in fuel assemblies to be used at the V.C Summer plant, calculations have been performed to determine if any positive reactivity effect is associated with the use of Erbium bearing rods in the PWR assemblies. Comparison of an assembly

without Erbia rods to assemblies with various numbers of Erbia rods at several loadings show that assemblies with Erbia rods have a lower reactivity than those assemblies without Erbia rods. Therefore, the burnup versus enrichment curve in Section 4.2.1.2 is applicable to assemblies either with or without Erbia rods.

4.4.8 MCNP4a Temperature Correction

The calculations performed using CASMO-4 are valid at 4° C and the temperature may be dictated by the code user. However, since the Doppler treatment and cross-sections in MCNP4a are valid only at 20° C, the Δk determined in CASMO-4 from 20° C to 4° C must be included in the final k_{eff} calculation.

Therefore the Δk is included as a bias in the final k_{eff} calculation in Tables 4.2.1 and 4.2.2.

4.4.9 Long-Term Changes in Reactivity

At reactor shutdown, the reactivity of the fuel initially decreases due to the growth of Xe-135. Subsequently, the Xenon decays and the reactivity increases to a maximum at several hundred hours when the Xenon is gone. Therefore, for conservatism, the Xe is set to zero in the calculations to assure maximum reactivity. During the next 50 years, the reactivity continuously decreases due primarily to ^{241}Pu decay and ^{241}Am growth. No credit is taken for this long-term decrease in reactivity other than to indicate additional and increasing subcriticality margin.

4.5 Region 1 Criticality Analyses and Tolerances

4.5.1 Nominal Design Case

For the nominal storage cell design in Region 1, the criticality safety analyses are summarized in Table 4.2.1. These data confirm that the maximum reactivity in Region 1 remains conservatively less than the regulatory limit ($k_{\text{eff}} \leq 0.95$). An independent calculation with the KENO5a code provides confirmation of the validity of the reference MCNP4a calculations.

4.5.2 Uncertainties Due to Burnup

For storage in Region 1, consideration of fuel burnup is not necessary, and thus, burnup related uncertainties are not applicable.

4.5.3 Uncertainties Due to Tolerances

The reactivity effects of manufacturing tolerances are tabulated, along with the tolerances, in Table 4.5.1. The individual tolerances were calculated for the design basis fresh unburned fuel assembly.

4.5.4 Eccentric Fuel Positioning

The fuel assembly is assumed to be normally located in the center of the storage rack cell. However, calculations were also made with the fuel assemblies assumed to be in the corner of the storage rack cell (four-assembly cluster at closest approach). These calculations indicated that the reactivity effect is small and negative. Therefore, the reference case in which the fuel assemblies are centered is bounding and no uncertainty for eccentricity is necessary.

4.5.5 Water-Gap Spacing Between Racks

The Boral panels installed on the external surfaces of interfacing Region 1 and Region 2 racks and the minimum water-gap spacing between racks, which is at least 2.0 inches between neighboring Region 1 style racks and also at least 2.0 inches between Region 1 and Region 2 style racks, constitutes a neutron flux-trap between the storage cells of facing racks. The racks are constructed with the base plates extending beyond the edge of the cells which assures that the minimum spacing between storage racks is maintained under all credible conditions. This water-gap flux-trap is larger than those between Region 1 cells (1.6 inches in both directions), and thus, will act to reduce the reactivity below the cited maximum.

4.6 Region 2 Criticality Analyses and Tolerances

4.6.1 Nominal Design Case

For the nominal storage cell design in Region 2, the criticality safety analyses are summarized in Table 4.2.2. These data confirm that the maximum reactivity in Region 2 remains conservatively less than the regulatory limit ($k_{\text{eff}} \leq 0.95$). An independent calculation with the KENO5a code provides confirmation of the validity of the reference MCNP4a calculations.

4.6.2 Uncertainties Due to Burnup

CASMO-4 was used for the depletion analysis and the restart option was used to analytically transfer the spent fuel into the storage rack configuration at a reference temperature of 4°C (corresponding to the highest reactivity, see Section 4.7.1). Calculations were also made for fuel of several different initial enrichments and interpolated to define the burnup-dependent equivalent enrichments³, at each burnup. MCNP4a calculations were then made for the equivalent enrichment to establish the limiting k_{eff} value, which includes all applicable uncertainties and the effect of the axial burnup distribution. These calculations were used to define the boundary of the acceptable domain shown in Figure 4.1.1.

4.6.3 Uncertainties Due to Tolerances

The reactivity effects of manufacturing tolerances are tabulated, along with the tolerances, in Table 4.6.1. All of the individual reactivity allowances were calculated for the reference fuel assembly at zero burnup and at burnups enveloping the criteria for storage (i.e., 35, 40, and 45 GWD/MTU). The largest statistical combination of uncertainties from either the fresh or burned condition was conservatively used.

³ The (reactivity) equivalent enrichment is the fresh un-burned fuel enrichment that yields the same reactivity as the depleted fuel, both evaluated in the storage rack configuration. The equivalent enrichment may then be used in three-dimensional MCNP4a or KENO5a calculations.

4.6.4 Eccentric Fuel Positioning

The fuel assembly is assumed to be normally located in the center of the storage rack cell. However, calculations were also made with the fuel assemblies assumed to be in the corner of the storage rack cell (four-assembly cluster at closest approach). These calculations indicated that the reactivity effect is small and negative. Therefore, the reference case in which the fuel assemblies are centered is bounding and no uncertainty for eccentricity is necessary.

4.6.5 Water-Gap Spacing Between Racks

The minimum water-gap between racks, which is 1.0 inch between neighboring Region 2 style racks and at least 2.0 inches between Region 1 and Region 2 style racks, constitutes a neutron flux-trap for the storage cells of facing racks. The racks are constructed with the base plates extending beyond the edge of the cells which assures that the minimum spacing between storage racks is maintained under all credible conditions. Region 2 style racks do not contain internal water gaps, and thus, this water-gap flux-trap will act to reduce the reactivity below the cited maximum.

4.7 Abnormal and Accident Conditions

4.7.1 Temperature and Water Density Effects

The moderator temperature coefficient of reactivity in both Region 1 and Region 2 is negative. Therefore, a moderator temperature of 4°C (39.2°F) was assumed for the reference calculations, which assures that the true reactivity will always be lower over the expected range of water temperatures. Temperature effects on reactivity have been evaluated (CASMO-4) and the results are shown in Table 4.7.1. In addition, the introduction of voids in the water internal to the storage cell (to simulate boiling) decreased reactivity, as shown in Table 4.7.1.

With soluble boron present, the temperature coefficients of reactivity would differ from those listed in Table 4.7.1. However, the reactivities would also be substantially lower at all temperatures with soluble boron present. The data in Table 4.7.1 are pertinent to the higher-reactivity unborated case.

4.7.2 Lateral Rack Movement

Lateral motion of the storage racks under seismic conditions could potentially alter the spacing between racks. In Region 1, the water gap between racks (at least 2.0 inches, as limited by the base plate extensions) is larger than the corresponding design water-gap spacing (1.6 inches in both directions) internal to the racks. Similarly, the water gap in the interface between Region 1 and Region 2 style racks (at least 2.00 inches, as limited by the base plate extensions) is also larger than the water gap internal to the Region 1 racks and Boral panels are installed on the external surfaces of interfacing Region 1 and Region 2 racks. Consequently, there will be no positive effect on reactivity as a result of lateral rack movement.

Region 2 storage cells do not use a flux-trap, and thus, the calculated maximum reactivity does not rely on spacing between racks. Nevertheless, the minimum water gap between Region 2 racks (1.0 inches, as limited by the base plate extensions) and the Boral panels, which are installed on one side of neighboring Region 2 racks, assure that the reactivity is always less than the design limitation. Furthermore, soluble poison would assure that a reactivity less than the design limitation is maintained under seismic conditions. Consequently, there will be no positive effect on reactivity as a result of lateral rack movement.

4.7.3 Abnormal Location of a Fuel Assembly

The misplacement of a fresh unburned fuel assembly could, in the absence of soluble poison, result in exceeding the regulatory limit ($k_{\text{eff}} \leq 0.95$). This could occur if a fresh fuel assembly of the highest permissible nominal initial enrichment (4.95 wt% ^{235}U) were to be inadvertently loaded into a Region 2 storage cell. Calculations confirmed that the highest reactivity, including uncertainties, for the worst case postulated accident condition (fresh fuel assembly in Region 2) would exceed the limit on reactivity in the

absence of soluble boron. Soluble boron in the spent fuel pool water, for which credit is permitted under these accident conditions, would assure that the reactivity is maintained substantially less than the design limitation. Calculations indicate that a soluble boron concentration of 347 ppm is adequate to assure that the maximum k_{eff} does not exceed 0.95.

In addition, the mislocation of a fresh unburned fuel assembly could, in the absence of soluble poison, result in exceeding the regulatory limit (k_{eff} of 0.95). This could possibly occur if a fresh fuel assembly of the highest permissible nominal initial enrichment (4.95 wt%) were to be accidentally mislocated outside of a Region 2 storage rack adjacent to other fuel assemblies. There is no area in the pool layout in which such an accident condition could be postulated to occur after all the racks are placed in the pool, as the gaps between racks and the spent fuel pool wall are sufficiently small to preclude the accidental mislocation of a fuel assembly outside of a storage rack. However, such a mislocation accident could occur during rack installation, where a fresh fuel assembly is placed outside and adjacent to the Region 2 rack, without a Boral panel between the fresh misplaced assembly and the burned assembly in the rack. Calculations confirmed that the highest reactivity, including uncertainties, for the worst case postulated accident condition (fresh fuel assembly adjacent to the filled Region 2 rack) would exceed the limit on reactivity in the absence of soluble boron. Soluble boron in the spent fuel pool water, for which credit is permitted under these accident conditions, would assure that the reactivity is maintained substantially less than the design limitation. Calculations indicate that a soluble boron concentration of 408 ppm is adequate to assure that the maximum k_{eff} does not exceed 0.95.

4.7.4 Dropped Fuel Assembly

For the case in which a fuel assembly is assumed to be dropped on top of a rack, the fuel assembly will come to rest horizontally on top of the rack with a minimum separation distance from the active fuel region of more than 12 inches, which is sufficient to preclude neutron coupling (i.e., an effectively infinite separation). Maximum expected deformation under seismic or accident conditions will not reduce the minimum spacing to less than 12 inches. Consequently, the horizontal fuel assembly drop accident will not result in a significant increase in reactivity. Furthermore, the soluble boron in the spent fuel pool water assures that the true reactivity is always less than the limiting value for this dropped fuel accident.

It is also possible to vertically drop an assembly into a location occupied by another assembly. Such a vertical impact, would, at most cause a small compression of the stored assembly, reducing the water-to-fuel ratio and thereby reducing reactivity. In addition the distance between the active fuel regions of both assemblies will be more than sufficient to ensure no neutron interaction between the two assemblies.

Structural analysis has shown that dropping an assembly into an unoccupied cell could result in a localized deformation of the baseplate of the rack. The resultant effect would be the lowering of a single fuel assembly by the amount of the deformation. This could potentially result in the active fuel height of that assembly no longer being completely covered by the Boral. The immediate eight surrounding fuel cells could also be affected. However, the amount of deformation for these cells would be considerably less. Structural analysis has shown that the amount of localized deformation will not exceed three inches. The reactivity consequence of this situation was calculated and found to be statistically insignificant. For simplicity in modeling, the calculation conservatively assumed an infinite array of assemblies in this damaged condition, and demonstrated the reactivity effect to be negligible. Since this is a localized event (nine storage cells at most) the actual reactivity effect will be even less than the calculated value. Furthermore, the soluble boron in the pool water assures that the true reactivity is always less than the limiting value for this dropped fuel accident.

4.8 References for Section 4.0

- [4.1.1] M. G. Natrella, Experimental Statistics, National Bureau of Standards Handbook 91, August 1963.
- [4.1.2] L.I. Kopp, "Guidance on the Regulatory Requirements for Criticality Analysis of Fuel Storage at Light-Water Reactor Power Plants," NRC Memorandum from L. Kopp to T. Collins, August 19, 1998.
- [4.4.1] J.F. Briesmeister, Editor, "MCNP - A General Monte Carlo N-Particle Transport Code, Version 4A," LA-12625, Los Alamos National Laboratory (1993).
- [4.4.2] L.M. Petrie and N.F. Landers, "KENO Va - An Improved Monte Carlo Criticality Program with Supergrouping," Volume 2, Section F11 from "SCALE: A Modular System for Performing Standardized Computer Analysis for Licensing Evaluation" NUREG/CR-0200, Rev. 4, January 1990.
- [4.4.3] "SCALE 4.3: A Modular System for Performing Standardized Computer Analysis for Licensing Evaluation For Workstations and Personal Computers, Volume 0," CCC-545, ORNL-RSICC, Oak Ridge National Laboratory (1995).
- [4.4.4] N.M. Greene, L.M. Petrie and R.M. Westfall, "NITAWL-II: Scale System Module for Performing Shielding and Working Library Production," Volume 1, Section F1 from "SCALE: A Modular System for Performing Standardized Computer Analysis for Licensing Evaluation" NUREG/CR-0200, Rev. 4, January 1990.
- [4.4.5] M. Edenius, K. Ekberg, B.H. Forssén, and D. Knott, "CASMO-4 A Fuel Assembly Burnup Program User's Manual," Studsvik/SOA-95/1, Studsvik of America, Inc. and Studsvik Core Analysis AB (proprietary).

- [4.4.6] D. Knott, "CASMO-4 Benchmark Against Critical Experiments", SOA-94/13, Studsvik of America, Inc., (proprietary).
- [4.4.7] D. Knott, "CASMO-4 Benchmark Against MCNP," SOA-94/12, Studsvik of America, Inc., (proprietary).
- [4.4.8] S.E. Turner, "Uncertainty Analysis - Burnup Distributions", presented at the DOE/SANDIA Technical Meeting on Fuel Burnup Credit, Special Session, ANS/ENS Conference, Washington, D.C., November 2, 1988.

Table 4.1.1
Fuel Assembly Specifications

Fuel Rod Data		
Assembly type	Westinghouse Vantage5 / Performance	Westinghouse Standard
Fuel pellet outside diameter, in.	0.3088	0.3225
Cladding thickness, in.	0.0225	0.0225
Cladding outside diameter, in.	0.360	0.374
Cladding material	Zr	Zr
Nominal Pellet density, g/cc	10.631	10.412 ⁴
Maximum enrichment, wt% ²³⁵ U	4.95 ± 0.05	4.95 ± 0.05
Fuel Assembly Data		
Fuel rod array	17 x 17	17 x 17
Number of fuel rods	264	264
Fuel rod pitch, in.	0.496	0.496
Number of control rod guide and instrument thimbles	25	25
Thimble outside diameter, in.	0.474	0.482
Thimble thickness, in.	0.016	0.016
Active fuel Length, in.	144	144

⁴ All calculations for the Westinghouse 17x17 Standard assembly and the Westinghouse 17x17 Vantage assembly were performed assuming a nominal *stack* density of 10.631 g/cc.

Table 4.2.1

Summary of the Criticality Safety Analyses for Region 1

Storage Arrangement	Unrestricted
Design Basis Burnup at 4.95 wt% ²³⁵ U	0
Uncertainties	
Bias Uncertainty (95%/95%)	± 0.0011
Calculational Statistics ⁵ (95%/95%, 2.0×σ)	± 0.0016
Depletion Uncertainty	N/A
Fuel Eccentricity	negative
Manufacturing Tolerances	± 0.0084
Statistical Combination of Uncertainties ⁶	± 0.0086
Reference k _{eff} (MCNP4a)	0.9222
Total Uncertainty (above)	0.0086
Axial Burnup Distribution	N/A
Temperature Δk	0.0016
Calculational Bias (see Appendix A)	0.0009
Maximum k_{eff}	0.9333⁷
Regulatory Limiting k_{eff}	0.9500

⁵ The value used for the MCNP4a (or KENO5a) statistical uncertainty is 2.0 times the estimated standard deviation. Each final k value calculated by MCNP4a (or KENO5a) is the result of averaging a minimum of 200 cycle k values, and thus, is based on a minimum sample size of 200. The K multiplier, for a one-sided statistical tolerance with 95% probability at the 95% confidence level, corresponding to a sample size of 200, is 1.84. However, for this analysis a value of 2.0 was assumed for the K multiplier, which is larger (more conservative) than the value corresponding to a sample size of 200.

⁶ Square root of the sum of the squares.

⁷ KENO5a verification calculation resulted in a maximum k_{eff} of 0.9309.

Table 4.2.2

Summary of the Criticality Safety Analyses for Region 2

Design Basis Burnup at 4.95 wt% ²³⁵ U	41.6 GWD/MTU
Uncertainties	
Bias Uncertainty (95%/95%)	± 0.0011
Calculational Statistics ⁸ (95%/95%, 2.0×σ)	± 0.0012
Depletion Uncertainty	± 0.0146
Fuel Eccentricity	negative
Manufacturing Tolerances	± 0.0055
Statistical Combination of Uncertainties ⁹	± 0.0157
Reference k _{eff} (MCNP4a)	0.9236
Total Uncertainty (above)	0.0157
Axial Burnup Distribution	0.0062
Temperature Δk	0.0021
Calculational Bias (see Appendix A)	0.0009
Maximum k_{eff}	0.9485¹⁰
Regulatory Limiting k_{eff}	0.9500

⁸The value used for the MCNP4a (or KENO5a) statistical uncertainty is 2.0 times the estimated standard deviation. Each final k value calculated by MCNP4a (or KENO5a) is the result of averaging a minimum of 200 cycle k values, and thus, is based on a minimum sample size of 200. The K multiplier, for a one-sided statistical tolerance with 95% probability at the 95% confidence level, corresponding to a sample size of 200, is 1.84. However, for this analysis a value of 2.0 was assumed for the K multiplier, which is larger (more conservative) than the value corresponding to a sample size of 200.

⁹Square root of the sum of the squares.

¹⁰KENO5a verification calculation resulted in a maximum k_{eff} of 0.9445.

Table 4.2.3

Burnup-Enrichment Limits in Region 2

Nominal Initial Fuel Enrichment (wt% ^{235}U)	Minimum Fuel Burnup (GWD/MTU)
2	4.940
2.5	12.052
3	18.678
3.5	24.908
4	30.838
4.5	36.561
5	41.611

Table 4.2.4

Reactivity Effects of Abnormal and Accident Conditions in Regions 1 and 2

Abnormal/Accident Conditions	Reactivity Effect
Temperature Increase (above 4°C)	Negative (Table 4.7.1)
Void (boiling)	Negative (Table 4.7.1)
Assembly Drop	Negligible
Lateral Rack Movement	Negligible
Misplacement of a Fresh Fuel Assembly in Region 2	Positive - controlled by a minimum of 400 ppm soluble boron
Mislocation of a Fresh Fuel Assembly outside Region 2	During Rack Installation Only – Positive – controlled by a minimum of 425 ppm soluble boron

Table 4.4.1

Reactivity of Assemblies Containing BPRAs

Group	# of Rods	Enrichment [wt% ²³⁵ U]	Cycle Burnup [GWD/MTU]	Assembly Burnup [GWD/MTU]	Rack k _{eff}
B	24	2.6	17.5	20	0.9165
C	24	3.1	17.5	25	0.9234
D	24	3.44	10	27.5	0.9286

Table 4.5.1

Reactivity Effects of Manufacturing Tolerances in Region 1

Tolerance	Reactivity Effect, Δk
Minimum Boral loading (nominal)	+0.0019
Minimum Boral width (nominal) ¹¹	+0.0006
Minimum Water Gap (nominal Water Gap) ¹²	+0.0077
Maximum box wall thickness (nominal)	+0.0004
Density tolerance (, 10.631 g/cm ³ nominal)	+0.0022
Enrichment (, 4.95 wt% ²³⁵ U nominal)	+0.0016
Total (statistical sum)¹³	+0.0084

¹¹ This is conservative as the specified minimum width of the Boral (including tolerances) is modeled.

¹² This is the maximum possible change in the water gap, predicated on the box I.D. and pitch being manufactured at their greatest tolerance in opposition to each other (i.e. maximum box I.D. and minimum pitch).

¹³ Square root of the sum of the squares.

Table 4.6.1

Reactivity Effects of Manufacturing Tolerances in Region 2

Tolerance	Reactivity Effect, Δk
Minimum Boral loading ([REDACTED] nominal)	+0.0028
Minimum Boral width ([REDACTED] nominal) ¹⁴	+0.0008
Minimum box I.D. ([REDACTED] nominal) ¹⁵	+0.0011
Maximum box wall thickness ([REDACTED] nominal)	+0.0008
Density ([REDACTED], 10.631 g/cm ³ nominal)	+0.0030
Enrichment ([REDACTED], 4.95 wt% ²³⁵ U nominal)	+0.0032
Total (statistical sum)¹⁶	+0.0055

¹⁴ This is conservative as the specified minimum width of the Boral (including tolerances) is modeled.

¹⁵ As the box I.D. and pitch are interrelated, a change in one of these parameters will necessarily change the other parameter. Therefore a 0.04 change in the box I.D. results in a 0.04 change in the pitch.

¹⁶ Square root of the sum of the squares.

Table 4.7.1

Reactivity Effects of Temperature and Void in Regions 1 and 2

Case	Reactivity Effect, Δk	
	Region 1	Region 2
4°C (39°F)	reference	reference
20°C (68°F)	-0.0016	-0.0021
60°C (140°F)	-0.0088	-0.0094
80°C (176°F)	-0.0137	-0.0141
120°C (248°F)	-0.0256	-0.0251
120°C w/ 10% void	-0.0568	-0.0497
120°C w/ 20% void	-0.0901	-0.0785
120°C w/ 30% void	-0.1255	-0.1125

Region II Racks Burnup vs. Enrichment Curve

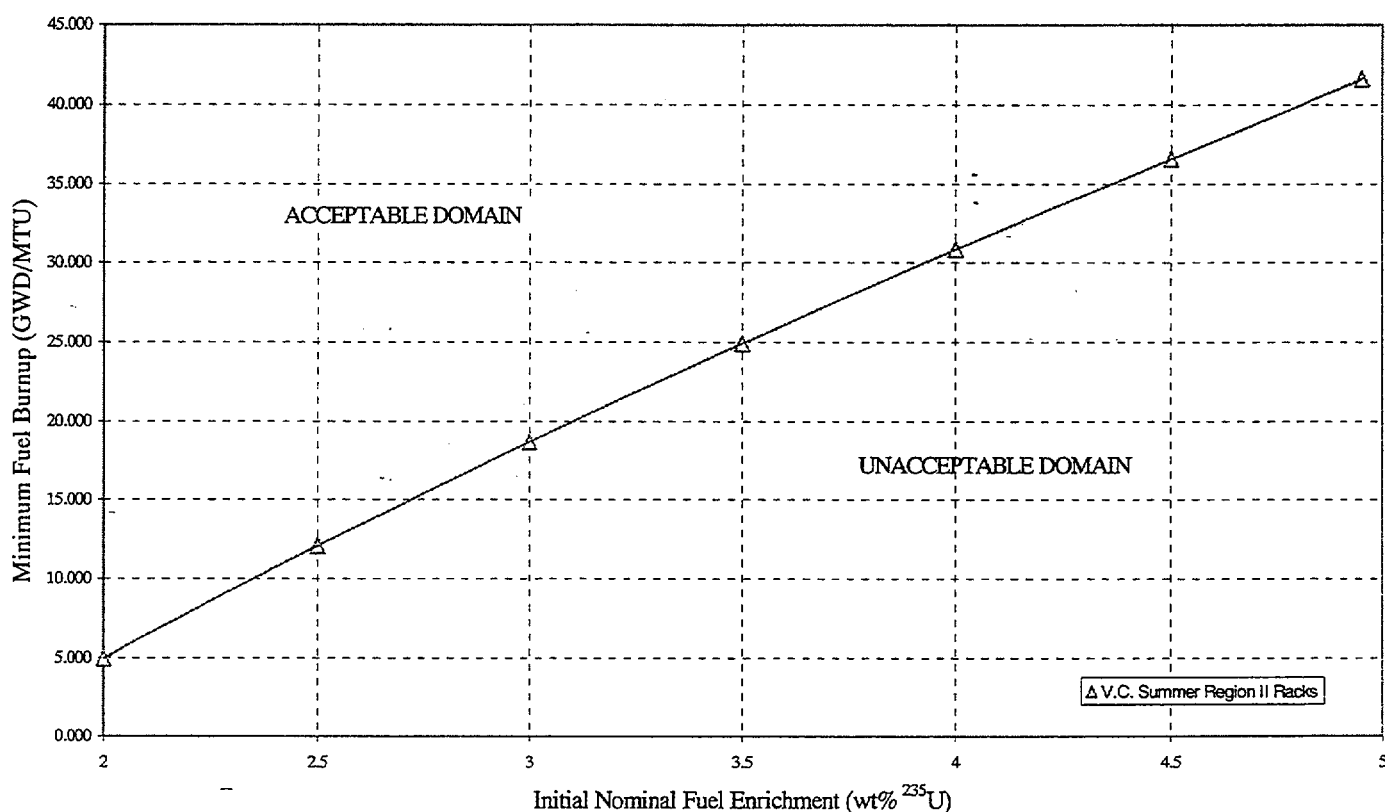


Figure 4.1.1: Minimum Required Fuel Assembly Burnup as a Function of Nominal Initial Enrichment to Permit Storage in Region 2 (Fuel assemblies with enrichments less than 2.0 wt% ²³⁵U will conservatively be required to meet the burnup requirements of 2.0 wt% ²³⁵U assemblies).¹⁷

¹⁷ Polynomial fit of the data is provided in Section 4.2.1.2. Burnup limits for nominal initial enrichments between 2.0 wt% ²³⁵U and 4.95 wt% ²³⁵U are provided in Table 4.2.3.

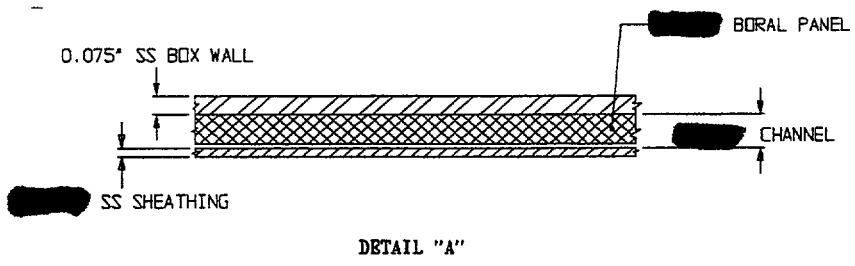
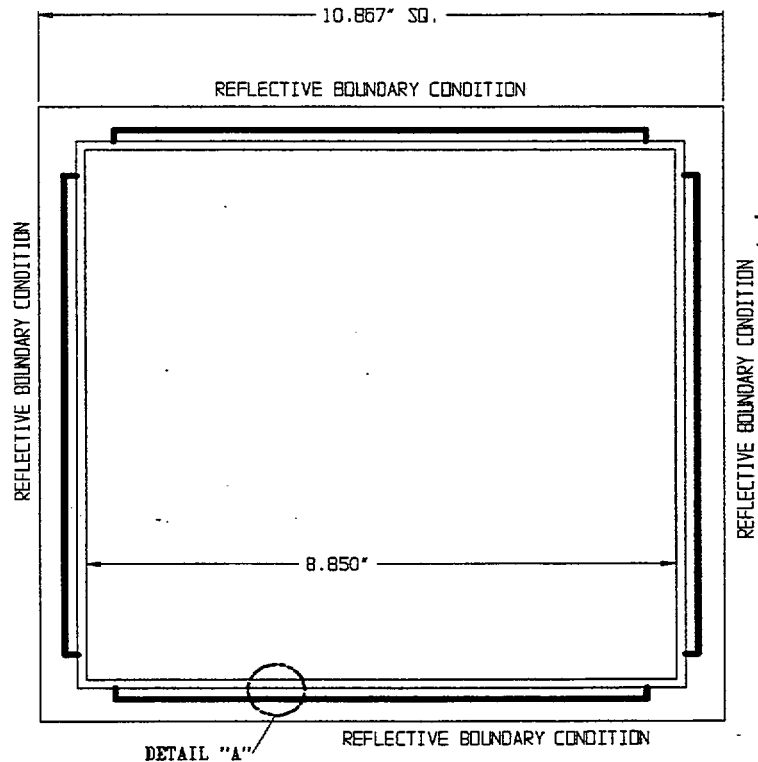


Figure 4.3.1: A Cross-Sectional View of the Computational Model Used for the Region I Rack Analysis (NOT TO SCALE).

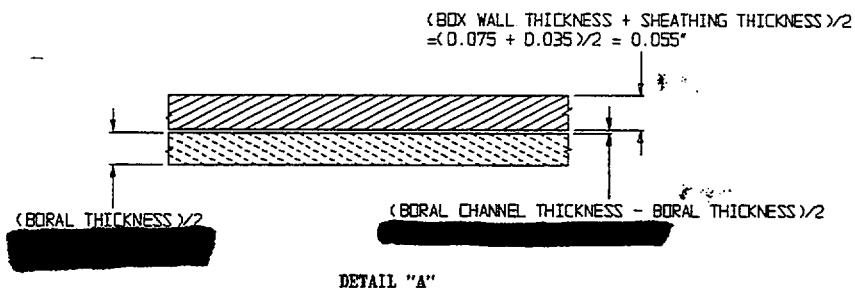
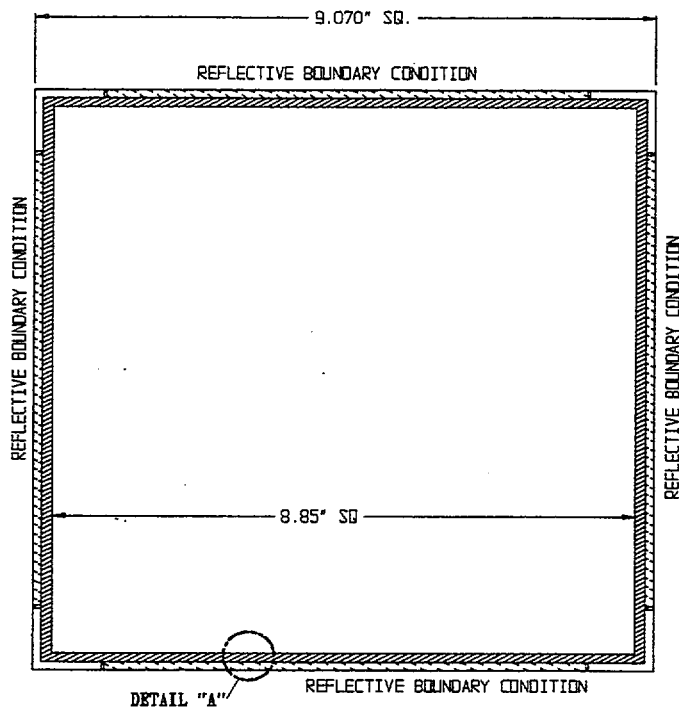


Figure 4.3.2: A Cross-Sectional View of the Calculational Model Used for the Region II Rack Analysis (NOT TO SCALE).

APPENDIX 4A: BENCHMARK CALCULATIONS

4A.1 INTRODUCTION AND SUMMARY

Benchmark calculations have been made on selected critical experiments, chosen, in so far as possible, to bound the range of variables in the rack designs. Two independent methods of analysis were used, differing in cross section libraries and in the treatment of the cross sections. MCNP4a [4A.1] is a continuous energy Monte Carlo code and KENO5a [4A.2] uses group-dependent cross sections. For the KENO5a analyses reported here, the 238-group library was chosen, processed through the NITAWL-II [4A.2] program to create a working library and to account for resonance self-shielding in uranium-238 (Nordheim integral treatment). The 238 group library was chosen to avoid or minimize the errors[†] (trends) that have been reported (e.g., [4A.3 through 4A.5]) for calculations with collapsed cross section sets.

In rack designs, the three most significant parameters affecting criticality are (1) the fuel enrichment, (2) the ¹⁰B loading in the neutron absorber, and (3) the lattice spacing (or water-gap thickness if a flux-trap design is used). Other parameters, within the normal range of rack and fuel designs, have a smaller effect, but are also included in the analyses.

Table 4A.1 summarizes results of the benchmark calculations for all cases selected and analyzed, as referenced in the table. The effect of the major variables are discussed in subsequent sections below. It is important to note that there is obviously considerable overlap in parameters since it is not possible to vary a single parameter and maintain criticality; some other parameter or parameters must be concurrently varied to maintain criticality.

One possible way of representing the data is through a spectrum index that incorporates all of the variations in parameters. KENO5a computes and prints the "energy of the average lethargy causing fission" (EALF). In MCNP4a, by utilizing the tally option with the identical 238-group energy structure as in KENO5a, the number of fissions in each group may be collected and the EALF determined (post-processing).

[†] Small but observable trends (errors) have been reported for calculations with the 27-group and 44-group collapsed libraries. These errors are probably due to the use of a single collapsing spectrum when the spectrum should be different for the various cases analyzed, as evidenced by the spectrum indices.

Figures 4A.1 and 4A.2 show the calculated k_{eff} for the benchmark critical experiments as a function of the EALF for MCNP4a and KENO5a, respectively (UO₂ fuel only). The scatter in the data (even for comparatively minor variation in critical parameters) represents experimental error[†] in performing the critical experiments within each laboratory, as well as between the various testing laboratories. The B&W critical experiments show a larger experimental error than the PNL criticals. This would be expected since the B&W criticals encompass a greater range of critical parameters than the PNL criticals.

Linear regression analysis of the data in Figures 4A.1 and 4A.2 show that there are no trends, as evidenced by very low values of the correlation coefficient (0.13 for MCNP4a and 0.21 for KENO5a). The total bias (systematic error, or mean of the deviation from a k_{eff} of exactly 1.000) for the two methods of analysis are shown in the table below.

Calculational Bias of MCNP4a and KENO5a	
MCNP4a	0.0009±0.0011
KENO5a	0.0030±0.0012

The bias and standard error of the bias were derived directly from the calculated k_{eff} values in Table 4A.1 using the following equations^{††}, with the standard error multiplied by the one-sided K-factor for 95% probability at the 95% confidence level from NBS Handbook 91 [4A.18] (for the number of cases analyzed, the K-factor is -2.05 or slightly more than 2).

$$\bar{k} = \frac{1}{n} \sum_i^n k_i \quad (4A.1)$$

[†] A classical example of experimental error is the corrected enrichment in the PNL experiments, first as an addendum to the initial report and, secondly, by revised values in subsequent reports for the same fuel rods.

^{††} These equations may be found in any standard text on statistics, for example, reference [4A.6] (or the MCNP4a manual) and is the same methodology used in MCNP4a and in KENO5a.

$$\sigma_{\bar{k}}^2 = \frac{\sum_{i=1}^n k_i^2 - (\sum_{i=1}^n k_i)^2 / n}{n(n-1)} \quad (4A.2)$$

$$Bias = (1 - \bar{k}) \pm K \sigma_{\bar{k}} \quad (4A.3)$$

where k_i are the calculated reactivities of n critical experiments; $\sigma_{\bar{k}}$ is the unbiased estimator of the standard deviation of the mean (also called the standard error of the bias (mean)); K is the one-sided multiplier for 95% probability at the 95% confidence level (NBS Handbook 91 [4A.18]).

Formula 4.A.3 is based on the methodology of the National Bureau of Standards (now NIST) and is used to calculate the values presented on page 4.A-2. The first portion of the equation, $(1 - \bar{k})$, is the actual bias which is added to the MCNP4a and KENO5a results. The second term, $K \sigma_{\bar{k}}$, is the uncertainty or standard error associated with the bias. The K values used were obtained from the National Bureau of Standards Handbook 91 and are for one-sided statistical tolerance limits for 95% probability at the 95% confidence level. The actual K values for the 56 critical experiments evaluated with MCNP4a and the 53 critical experiments evaluated with KENO5a are 2.04 and 2.05, respectively.

The bias values are used to evaluate the maximum k_{eff} values for the rack designs. KENO5a has a slightly larger systematic error than MCNP4a, but both result in greater precision than published data [4A.3 through 4A.5] would indicate for collapsed cross section sets in KENO5a (SCALE) calculations.

4A.2 Effect of Enrichment

The benchmark critical experiments include those with enrichments ranging from 2.46 w/o to 5.74 w/o and therefore span the enrichment range for rack designs. Figures 4A.3 and 4A.4 show the calculated k_{eff} values (Table 4A.1) as a function of the fuel enrichment reported for the critical experiments. Linear regression analyses for these data confirms that there are no trends, as indicated by low values of the correlation coefficients (0.03 for MCNP4a and 0.38 for KENO5a). Thus, there are no corrections to the bias for the various enrichments.

As further confirmation of the absence of any trends with enrichment, a typical configuration was calculated with both MCNP4a and KENO5a for various enrichments. The cross-comparison of calculations with codes of comparable sophistication is suggested in Reg. Guide 3.41. Results of this comparison, shown in Table 4A.2 and Figure 4A.5, confirm no significant difference in the calculated values of k_{eff} for the two independent codes as evidenced by the 45° slope of the curve. Since it is very unlikely that two independent methods of analysis would be subject to the same error, this comparison is considered confirmation of the absence of an enrichment effect (trend) in the bias.

4A.3 Effect of ^{10}B Loading

Several laboratories have performed critical experiments with a variety of thin absorber panels similar to the Boral panels in the rack designs. Of these critical experiments, those performed by B&W are the most representative of the rack designs. PNL has also made some measurements with absorber plates, but, with one exception (a flux-trap experiment), the reactivity worth of the absorbers in the PNL tests is very low and any significant errors that might exist in the treatment of strong thin absorbers could not be revealed.

Table 4A.3 lists the subset of experiments using thin neutron absorbers (from Table 4A.1) and shows the reactivity worth (Δk) of the absorber.[†]

No trends with reactivity worth of the absorber are evident, although based on the calculations shown in Table 4A.3, some of the B&W critical experiments seem to have unusually large experimental errors. B&W made an effort to report some of their experimental errors. Other laboratories did not evaluate their experimental errors.

To further confirm the absence of a significant trend with ^{10}B concentration in the absorber, a cross-comparison was made with MCNP4a and KENO5a (as suggested in Reg. Guide 3.41). Results are shown in Figure 4A.6 and Table 4A.4 for a typical geometry. These data substantiate the absence of any error (trend) in either of the two codes for the conditions analyzed (data points fall on a 45° line, within an expected 95% probability limit).

[†] The reactivity worth of the absorber panels was determined by repeating the calculation with the absorber analytically removed and calculating the incremental (Δk) change in reactivity due to the absorber.

4A.4 Miscellaneous and Minor Parameters

4A.4.1 Reflector Material and Spacings

PNL has performed a number of critical experiments with thick steel and lead reflectors.[†] Analysis of these critical experiments are listed in Table 4A.5 (subset of data in Table 4A.1). There appears to be a small tendency toward overprediction of k_{eff} at the lower spacing, although there are an insufficient number of data points in each series to allow a quantitative determination of any trends. The tendency toward overprediction at close spacing means that the rack calculations may be slightly more conservative than otherwise.

4A.4.2 Fuel Pellet Diameter and Lattice Pitch

The critical experiments selected for analysis cover a range of fuel pellet diameters from 0.311 to 0.444 inches, and lattice spacings from 0.476 to 1.00 inches. In the rack designs, the fuel pellet diameters range from 0.303 to 0.3805 inches O.D. (0.496 to 0.580 inch lattice spacing) for PWR fuel and from 0.3224 to 0.494 inches O.D. (0.488 to 0.740 inch lattice spacing) for BWR fuel. Thus, the critical experiments analyzed provide a reasonable representation of power reactor fuel. Based on the data in Table 4A.1, there does not appear to be any observable trend with either fuel pellet diameter or lattice pitch, at least over the range of the critical experiments applicable to rack designs.

4A.4.3 Soluble Boron Concentration Effects

Various soluble boron concentrations were used in the B&W series of critical experiments and in one PNL experiment, with boron concentrations ranging up to 2550 ppm. Results of MCNP4a (and one KENO5a) calculations are shown in Table 4A.6. Analyses of the very high boron concentration experiments (> 1300 ppm) show a tendency to slightly overpredict reactivity for the three experiments exceeding 1300 ppm. In turn, this would suggest that the evaluation of the racks with higher soluble boron concentrations could be slightly conservative.

[†] Parallel experiments with a depleted uranium reflector were also performed but not included in the present analysis since they are not pertinent to the Holtec rack design.

The number of critical experiments with PuO₂ bearing fuel (MOX) is more limited than for UO₂ fuel. However, a number of MOX critical experiments have been analyzed and the results are shown in Table 4A.7. Results of these analyses are generally above a k_{eff} of 1.00, indicating that when Pu is present, both MCNP4a and KENO5a overpredict the reactivity. This may indicate that calculation for MOX fuel will be expected to be conservative, especially with MCNP4a. It may be noted that for the larger lattice spacings, the KENO5a calculated reactivities are below 1.00, suggesting that a small trend may exist with KENO5a. It is also possible that the overprediction in k_{eff} for both codes may be due to a small inadequacy in the determination of the Pu-241 decay and Am-241 growth. This possibility is supported by the consistency in calculated k_{eff} over a wide range of the spectral index (energy of the average lethargy causing fission).

References

- [4A.1] J.F. Briesmeister, Ed., "MCNP4a - A General Monte Carlo N-Particle Transport Code, Version 4A; Los Alamos National Laboratory, LA-12625-M (1993).
- [4A.2] SCALE 4.3, "A Modular Code System for Performing Standardized Computer Analyses for Licensing Evaluation", NUREG-0200 (ORNL-NUREG-CSD-2/U2/R5, Revision 5, Oak Ridge National Laboratory, September 1995.
- [4A.3] M.D. DeHart and S.M. Bowman, "Validation of the SCALE Broad Structure 44-G Group ENDF/B-Y Cross-Section Library for Use in Criticality Safety Analyses", NUREG/CR-6102 (ORNL/TM-12460) Oak Ridge National Laboratory, September 1994.
- [4A.4] W.C. Jordan et al., "Validation of KENO.V.a", CSD/TM-238, Martin Marietta Energy Systems, Inc., Oak Ridge National Laboratory, December 1986.
- [4A.5] O.W. Hermann et al., "Validation of the Scale System for PWR Spent Fuel Isotopic Composition Analysis", ORNL-TM-12667, Oak Ridge National Laboratory, undated.
- [4A.6] R.J. Larsen and M.L. Marx, An Introduction to Mathematical Statistics and its Applications, Prentice-Hall, 1986.
- [4A.7] M.N. Baldwin et al., Critical Experiments Supporting Close Proximity Water Storage of Power Reactor Fuel, BAW-1484-7, Babcock and Wilcox Company, July 1979.
- [4A.8] G.S. Hoovier et al., Critical Experiments Supporting Underwater Storage of Tightly Packed Configurations of Spent Fuel Pins, BAW-1645-4, Babcock & Wilcox Company, November 1991.
- [4A.9] L.W. Newman et al., Urania Gadolinia: Nuclear Model Development and Critical Experiment Benchmark, BAW-1810, Babcock and Wilcox Company, April 1984.

- [4A.10] J.C. Manaranche et al., "Dissolution and Storage Experimental Program with 4.75 w/o Enriched Uranium-Oxide Rods," Trans. Am. Nucl. Soc. 33: 362-364 (1979).
- [4A.11] S.R. Bierman and E.D. Clayton, Criticality Experiments with Subcritical Clusters of 2.35 w/o and 4.31 w/o ^{235}U Enriched UO_2 Rods in Water with Steel Reflecting Walls, PNL-3602, Battelle Pacific Northwest Laboratory, April 1981.
- [4A.12] S.R. Bierman et al., Criticality Experiments with Subcritical Clusters of 2.35 w/o and 4.31 w/o ^{235}U Enriched UO_2 Rods in Water with Uranium or Lead Reflecting Walls, PNL-3926, Battelle Pacific Northwest Laboratory, December, 1981.
- [4A.13] S.R. Bierman et al., Critical Separation Between Subcritical Clusters of 4.31 w/o ^{235}U Enriched UO_2 Rods in Water with Fixed Neutron Poisons, PNL-2615, Battelle Pacific Northwest Laboratory, October 1977.
- [4A.14] S.R. Bierman, Criticality Experiments with Neutron Flux Traps Containing Voids, PNL-7167, Battelle Pacific Northwest Laboratory, April 1990.
- [4A.15] B.M. Durst et al., Critical Experiments with 4.31 wt % ^{235}U Enriched UO_2 Rods in Highly Borated Water Lattices, PNL-4267, Battelle Pacific Northwest Laboratory, August 1982.
- [4A.16] S.R. Bierman, Criticality Experiments with Fast Test Reactor Fuel Pins in Organic Moderator, PNL-5803, Battelle Pacific Northwest Laboratory, December 1981.
- [4A.17] E.G. Taylor et al., Saxton Plutonium Program Critical Experiments for the Saxton Partial Plutonium Core, WCAP-3385-54, Westinghouse Electric Corp., Atomic Power Division, December 1965.
- [4A.18] M.G. Natrella, Experimental Statistics, National Bureau of Standards, Handbook 91, August 1963.

Table 4A.1

Summary of Criticality Benchmark Calculations

Reference	Identification	Enrich.	Calculated k_{eff}		EALF [†] (eV)		
			MCNP4a	KENO5a	MCNP4a	KENO5a	
1	B&W-1484 (4A.7)	Core I	2.46	0.9964 ± 0.0010	0.9898 ± 0.0006	0.1759	0.1753
2	B&W-1484 (4A.7)	Core II	2.46	1.0008 ± 0.0011	1.0015 ± 0.0005	0.2553	0.2446
3	B&W-1484 (4A.7)	Core III	2.46	1.0010 ± 0.0012	1.0005 ± 0.0005	0.1999	0.1939
4	B&W-1484 (4A.7)	Core IX	2.46	0.9956 ± 0.0012	0.9901 ± 0.0006	0.1422	0.1426
5	B&W-1484 (4A.7)	Core X	2.46	0.9980 ± 0.0014	0.9922 ± 0.0006	0.1513	0.1499
6	B&W-1484 (4A.7)	Core XI	2.46	0.9978 ± 0.0012	1.0005 ± 0.0005	0.2031	0.1947
7	B&W-1484 (4A.7)	Core XII	2.46	0.9988 ± 0.0011	0.9978 ± 0.0006	0.1718	0.1662
8	B&W-1484 (4A.7)	Core XIII	2.46	1.0020 ± 0.0010	0.9952 ± 0.0006	0.1988	0.1965
9	B&W-1484 (4A.7)	Core XIV	2.46	0.9953 ± 0.0011	0.9928 ± 0.0006	0.2022	0.1986
10	B&W-1484 (4A.7)	Core XV ^{††}	2.46	0.9910 ± 0.0011	0.9909 ± 0.0006	0.2092	0.2014
11	B&W-1484 (4A.7)	Core XVI ^{††}	2.46	0.9935 ± 0.0010	0.9889 ± 0.0006	0.1757	0.1713
12	B&W-1484 (4A.7)	Core XVII	2.46	0.9962 ± 0.0012	0.9942 ± 0.0005	0.2083	0.2021
13	B&W-1484 (4A.7)	Core XVIII	2.46	1.0036 ± 0.0012	0.9931 ± 0.0006	0.1705	0.1708

Table 4A.1

Summary of Criticality Benchmark Calculations

Reference	Identification	Enrich.	Calculated k_{eff}		EALF [†] (eV)		
			MCNP4a	KENO5a	MCNP4a	KENO5a	
14	B&W-1484 (4A.7)	Core XIX	2.46	0.9961 ± 0.0012	0.9971 ± 0.0005	0.2103	0.2011
15	B&W-1484 (4A.7)	Core XX	2.46	1.0008 ± 0.0011	0.9932 ± 0.0006	0.1724	0.1701
16	B&W-1484 (4A.7)	Core XXI	2.46	0.9994 ± 0.0010	0.9918 ± 0.0006	0.1544	0.1536
17	B&W-1645 (4A.8)	S-type Fuel, w/886 ppm B	2.46	0.9970 ± 0.0010	0.9924 ± 0.0006	1.4475	1.4680
18	B&W-1645 (4A.8)	S-type Fuel, w/746 ppm B	2.46	0.9990 ± 0.0010	0.9913 ± 0.0006	1.5463	1.5660
19	B&W-1645 (4A.8)	SO-type Fuel, w/1156 ppm B	2.46	0.9972 ± 0.0009	0.9949 ± 0.0005	0.4241	0.4331
20	B&W-1810 (4A.9)	Case 1 1337 ppm B	2.46	1.0023 ± 0.0010	NC	0.1531	NC
21	B&W-1810 (4A.9)	Case 12 1899 ppm B	2.46/4.02	1.0060 ± 0.0009	NC	0.4493	NC
22	French (4A.10)	Water Moderator 0 gap	4.75	0.9966 ± 0.0013	NC	0.2172	NC
23	French (4A.10)	Water Moderator 2.5 cm gap	4.75	0.9952 ± 0.0012	NC	0.1778	NC
24	French (4A.10)	Water Moderator 5 cm gap	4.75	0.9943 ± 0.0010	NC	0.1677	NC
25	French (4A.10)	Water Moderator 10 cm gap	4.75	0.9979 ± 0.0010	NC	0.1736	NC
26	PNL-3602 (4A.11)	Steel Reflector, 0 separation	2.35	NC	1.0004 ± 0.0006	NC	0.1018

Table 4A.1
Summary of Criticality Benchmark Calculations

Reference	Identification	Enrich.	Calculated k_{eff}		EALF [†] (eV)		
			MCNP4a	KENO5a	MCNP4a	KENO5a	
27	PNL-3602 (4A.11)	Steel Reflector, 1.321 cm sepn.	2.35	0.9980 ± 0.0009	0.9992 ± 0.0006	0.1000	0.0909
28	PNL-3602 (4A.11)	Steel Reflector, 2.616 cm sepn	2.35	0.9968 ± 0.0009	0.9964 ± 0.0006	0.0981	0.0975
29	PNL-3602 (4A.11)	Steel Reflector, 3.912 cm sepn.	2.35	0.9974 ± 0.0010	0.9980 ± 0.0006	0.0976	0.0970
30	PNL-3602 (4A.11)	Steel Reflector, infinite sepn.	2.35	0.9962 ± 0.0008	0.9939 ± 0.0006	0.0973	0.0968
31	PNL-3602 (4A.11)	Steel Reflector, 0 cm sepn.	4.306	NC	1.0003 ± 0.0007	NC	0.3282
32	PNL-3602 (4A.11)	Steel Reflector, 1.321 cm sepn.	4.306	0.9997 ± 0.0010	1.0012 ± 0.0007	0.3016	0.3039
33	PNL-3602 (4A.11)	Steel Reflector, 2.616 cm sepn.	4.306	0.9994 ± 0.0012	0.9974 ± 0.0007	0.2911	0.2927
34	PNL-3602 (4A.11)	Steel Reflector, 5.405 cm sepn.	4.306	0.9969 ± 0.0011	0.9951 ± 0.0007	0.2828	0.2860
35	PNL-3602 (4A.11)	Steel Reflector, infinite sepn. ^{††}	4.306	0.9910 ± 0.0020	0.9947 ± 0.0007	0.2851	0.2864
36	PNL-3602 (4A.11)	Steel Reflector, with Boral Sheets	4.306	0.9941 ± 0.0011	0.9970 ± 0.0007	0.3135	0.3150
37	PNL-3926 (4A.12)	Lead Reflector, 0 cm sepn.	4.306	NC	1.0003 ± 0.0007	NC	0.3159
38	PNL-3926 (4A.12)	Lead Reflector, 0.55 cm sepn.	4.306	1.0025 ± 0.0011	0.9997 ± 0.0007	0.3030	0.3044
39	PNL-3926 (4A.12)	Lead Reflector, 1.956 cm sepn.	4.306	1.0000 ± 0.0012	0.9985 ± 0.0007	0.2883	0.2930

Table 4A.1
Summary of Criticality Benchmark Calculations

Reference	Identification	Enrich.	Calculated k_{eff}		EALF ¹ (eV)		
			MCNP4a	KENO5a	MCNP4a	KENO5a	
40	PNL-3926 (4A.12)	Lead Reflector, 5.405 cm sepn.	4.306	0.9971 ± 0.0012	0.9946 ± 0.0007	0.2831	0.2854
41	PNL-2615 (4A.13)	Experiment 004/032 - no absorber	4.306	0.9925 ± 0.0012	0.9950 ± 0.0007	0.1155	0.1159
42	PNL-2615 (4A.13)	Experiment 030 - Zr plates	4.306	NC	0.9971 ± 0.0007	NC	0.1154
43	PNL-2615 (4A.13)	Experiment 013 - Steel plates	4.306	NC	0.9965 ± 0.0007	NC	0.1164
44	PNL-2615 (4A.13)	Experiment 014 - Steel plates	4.306	NC	0.9972 ± 0.0007	NC	0.1164
45	PNL-2615 (4A.13)	Exp. 009 1.05% Boron-Steel plates	4.306	0.9982 ± 0.0010	0.9981 ± 0.0007	0.1172	0.1162
46	PNL-2615 (4A.13)	Exp. 012 1.62% Boron-Steel plates	4.306	0.9996 ± 0.0012	0.9982 ± 0.0007	0.1161	0.1173
47	PNL-2615 (4A.13)	Exp. 031 - Boral plates	4.306	0.9994 ± 0.0012	0.9969 ± 0.0007	0.1165	0.1171
48	PNL-7167 (4A.14)	Experiment 214R - with flux trap	4.306	0.9991 ± 0.0011	0.9956 ± 0.0007	0.3722	0.3812
49	PNL-7167 (4A.14)	Experiment 214V3 - with flux trap	4.306	0.9969 ± 0.0011	0.9963 ± 0.0007	0.3742	0.3826
50	PNL-4267 (4A.15)	Case 173 - 0 ppm B	4.306	0.9974 ± 0.0012	NC	0.2893	NC
51	PNL-4267 (4A.15)	Case 177 - 2550 ppm B	4.306	1.0057 ± 0.0010	NC	0.5509	NC
52	PNL-5803 (4A.16)	MOX Fuel - Type 3.2 Exp. 21	20% Pu	1.0041 ± 0.0011	1.0046 ± 0.0006	0.9171	0.8868

Table 4A.1

Summary of Criticality Benchmark Calculations

Reference	Identification	Enrich.	Calculated k_{eff}		EALF [†] (eV)		
			MCNP4a	KENO5a	MCNP4a	KENO5a	
53	PNL-5803 (4A.16)	MOX Fuel - Type 3.2 Exp. 43	20% Pu	1.0058 ± 0.0012	1.0036 ± 0.0006	0.2968	0.2944
54	PNL-5803 (4A.16)	MOX Fuel - Type 3.2 Exp. 13	20% Pu	1.0083 ± 0.0011	0.9989 ± 0.0006	0.1665	0.1706
55	PNL-5803 (4A.16)	MOX Fuel - Type 3.2 Exp. 32	20% Pu	1.0079 ± 0.0011	0.9966 ± 0.0006	0.1139	0.1165
56	WCAP-3385 (4A.17)	Saxton Case 52 PuO ₂ 0.52" pitch	6.6% Pu	0.9996 ± 0.0011	1.0005 ± 0.0006	0.8665	0.8417
57	WCAP-3385 (4A.17)	Saxton Case 52 U 0.52" pitch	5.74	1.0000 ± 0.0010	0.9956 ± 0.0007	0.4476	0.4580
58	WCAP-3385 (4A.17)	Saxton Case 56 PuO ₂ 0.56" pitch	6.6% Pu	1.0036 ± 0.0011	1.0047 ± 0.0006	0.5289	0.5197
59	WCAP-3385 (4A.17)	Saxton Case 56 borated PuO ₂	6.6% Pu	1.0008 ± 0.0010	NC	0.6389	NC
60	WCAP-3385 (4A.17)	Saxton Case 56 U 0.56" pitch	5.74	0.9994 ± 0.0011	0.9967 ± 0.0007	0.2923	0.2954
61	WCAP-3385 (4A.17)	Saxton Case 79 PuO ₂ 0.79" pitch	6.6% Pu	1.0063 ± 0.0011	1.0133 ± 0.0006	0.1520	0.1555
62	WCAP-3385 (4A.17)	Saxton Case 79 U 0.79" pitch	5.74	1.0039 ± 0.0011	1.0008 ± 0.0006	0.1036	0.1047

Notes: NC stands for not calculated.

† EALF is the energy of the average lethargy causing fission.

†† These experimental results appear to be statistical outliers ($> 3\sigma$) suggesting the possibility of unusually large experimental error. Although they could justifiably be excluded, for conservatism, they were retained in determining the calculational basis.

Table 4A.2

COMPARISON OF MCNP4a AND KENO5a CALCULATED REACTIVITIES[†]
FOR VARIOUS ENRICHMENTS

Enrichment	Calculated $k_{eff} \pm 1\sigma$	
	MCNP4a	KENO5a
3.0	0.8465 \pm 0.0011	0.8478 \pm 0.0004
3.5	0.8820 \pm 0.0011	0.8841 \pm 0.0004
3.75	0.9019 \pm 0.0011	0.8987 \pm 0.0004
4.0	0.9132 \pm 0.0010	0.9140 \pm 0.0004
4.2	0.9276 \pm 0.0011	0.9237 \pm 0.0004
4.5	0.9400 \pm 0.0011	0.9388 \pm 0.0004

[†] Based on the GE 8x8R fuel assembly.

Table 4A.3

**MCNP4a CALCULATED REACTIVITIES FOR
CRITICAL EXPERIMENTS WITH NEUTRON ABSORBERS**

Ref.	Experiment		Δk Worth of Absorber	MCNP4a Calculated k_{eff}	EALF [†] (eV)
4A.13	PNL-2615	Boral Sheet	0.0139	0.9994±0.0012	0.1165
4A.7	B&W-1484	Core XX	0.0165	1.0008±0.0011	0.1724
4A.13	PNL-2615	1.62% Boron-steel	0.0165	0.9996±0.0012	0.1161
4A.7	B&W-1484	Core XIX	0.0202	0.9961±0.0012	0.2103
4A.7	B&W-1484	Core XXI	0.0243	0.9994±0.0010	0.1544
4A.7	B&W-1484	Core XVII	0.0519	0.9962±0.0012	0.2083
4A.11	PNL-3602	Boral Sheet	0.0708	0.9941±0.0011	0.3135
4A.7	B&W-1484	Core XV	0.0786	0.9910±0.0011	0.2092
4A.7	B&W-1484	Core XVI	0.0845	0.9935±0.0010	0.1757
4A.7	B&W-1484	Core XIV	0.1575	0.9953±0.0011	0.2022
4A.7	B&W-1484	Core XIII	0.1738	1.0020±0.0011	0.1988
4A.14	PNL-7167	Expt 214R flux trap	0.1931	0.9991±0.0011	0.3722

[†]EALF is the energy of the average lethargy causing fission.

Table 4A.4

COMPARISON OF MCNP4a AND KENO5a
CALCULATED REACTIVITIES[†] FOR VARIOUS ¹⁰B LOADINGS

¹⁰ B, g/cm ²	Calculated $k_{eff} \pm 1\sigma$	
	MCNP4a	KENO5a
0.005	1.0381 ± 0.0012	1.0340 ± 0.0004
0.010	0.9960 ± 0.0010	0.9941 ± 0.0004
0.015	0.9727 ± 0.0009	0.9713 ± 0.0004
0.020	0.9541 ± 0.0012	0.9560 ± 0.0004
0.025	0.9433 ± 0.0011	0.9428 ± 0.0004
0.03	0.9325 ± 0.0011	0.9338 ± 0.0004
0.035	0.9234 ± 0.0011	0.9251 ± 0.0004
0.04	0.9173 ± 0.0011	0.9179 ± 0.0004

[†] Based on a 4.5% enriched GE 8x8R fuel assembly.

Table 4A.5

**CALCULATIONS FOR CRITICAL EXPERIMENTS WITH
THICK LEAD AND STEEL REFLECTORS[†]**

Ref.	Case	E, wt%	Separation, cm	MCNP4a k_{eff}	KENO5a k_{eff}
4A.11	Steel Reflector	2.35	1.321	0.9980 ± 0.0009	0.9992 ± 0.0006
		2.35	2.616	0.9968 ± 0.0009	0.9964 ± 0.0006
		2.35	3.912	0.9974 ± 0.0010	0.9980 ± 0.0006
		2.35	∞	0.9962 ± 0.0008	0.9939 ± 0.0006
4A.11	Steel Reflector	4.306	1.321	0.9997 ± 0.0010	1.0012 ± 0.0007
		4.306	2.616	0.9994 ± 0.0012	0.9974 ± 0.0007
		4.306	3.405	0.9969 ± 0.0011	0.9951 ± 0.0007
		4.306	∞	0.9910 ± 0.0020	0.9947 ± 0.0007
4A.12	Lead Reflector	4.306	0.55	1.0025 ± 0.0011	0.9997 ± 0.0007
		4.306	1.956	1.0000 ± 0.0012	0.9985 ± 0.0007
		4.306	5.405	0.9971 ± 0.0012	0.9946 ± 0.0007

[†] Arranged in order of increasing reflector-fuel spacing.

Table 4A.6

CALCULATIONS FOR CRITICAL EXPERIMENTS WITH VARIOUS SOLUBLE BORON CONCENTRATIONS

Reference	Experiment	Boron Concentration, ppm	Calculated k_{eff}	
			MCNP4a	KENO5a
4A.15	PNL-4267	0	0.9974 ± 0.0012	-
4A.8	B&W-1645	886	0.9970 ± 0.0010	0.9924 ± 0.0006
4A.9	B&W-1810	1337	1.0023 ± 0.0010	-
4A.9	B&W-1810	1899	1.0060 ± 0.0009	-
4A.15	PNL-4267	2550	1.0057 ± 0.0010	-

Table 4A.7

CALCULATIONS FOR CRITICAL EXPERIMENTS WITH MOX FUEL

Reference	Case [†]	MCNP4a		KENO5a	
		k_{eff}	EALF ^{††}	k_{eff}	EALF ^{††}
PNL-5803 [4A.16]	MOX Fuel - Exp. No. 21	1.0041±0.0011	0.9171	1.0046±0.0006	0.8868
	MOX Fuel - Exp. No. 43	1.0058±0.0012	0.2968	1.0036±0.0006	0.2944
	MOX Fuel - Exp. No. 13	1.0083±0.0011	0.1665	0.9989±0.0006	0.1706
	MOX Fuel - Exp. No. 32	1.0079±0.0011	0.1139	0.9966±0.0006	0.1165
WCAP-3385-54 [4A.17]	Saxton @ 0.52" pitch	0.9996±0.0011	0.8665	1.0005±0.0006	0.8417
	Saxton @ 0.56" pitch	1.0036±0.0011	0.5289	1.0047±0.0006	0.5197
	Saxton @ 0.56" pitch borated	1.0008±0.0010	0.6389	NC	NC
	Saxton @ 0.79" pitch	1.0063±0.0011	0.1520	1.0133±0.0006	0.1555

Note: NC stands for not calculated

† Arranged in order of increasing lattice spacing.

†† EALF is the energy of the average lethargy causing fission.

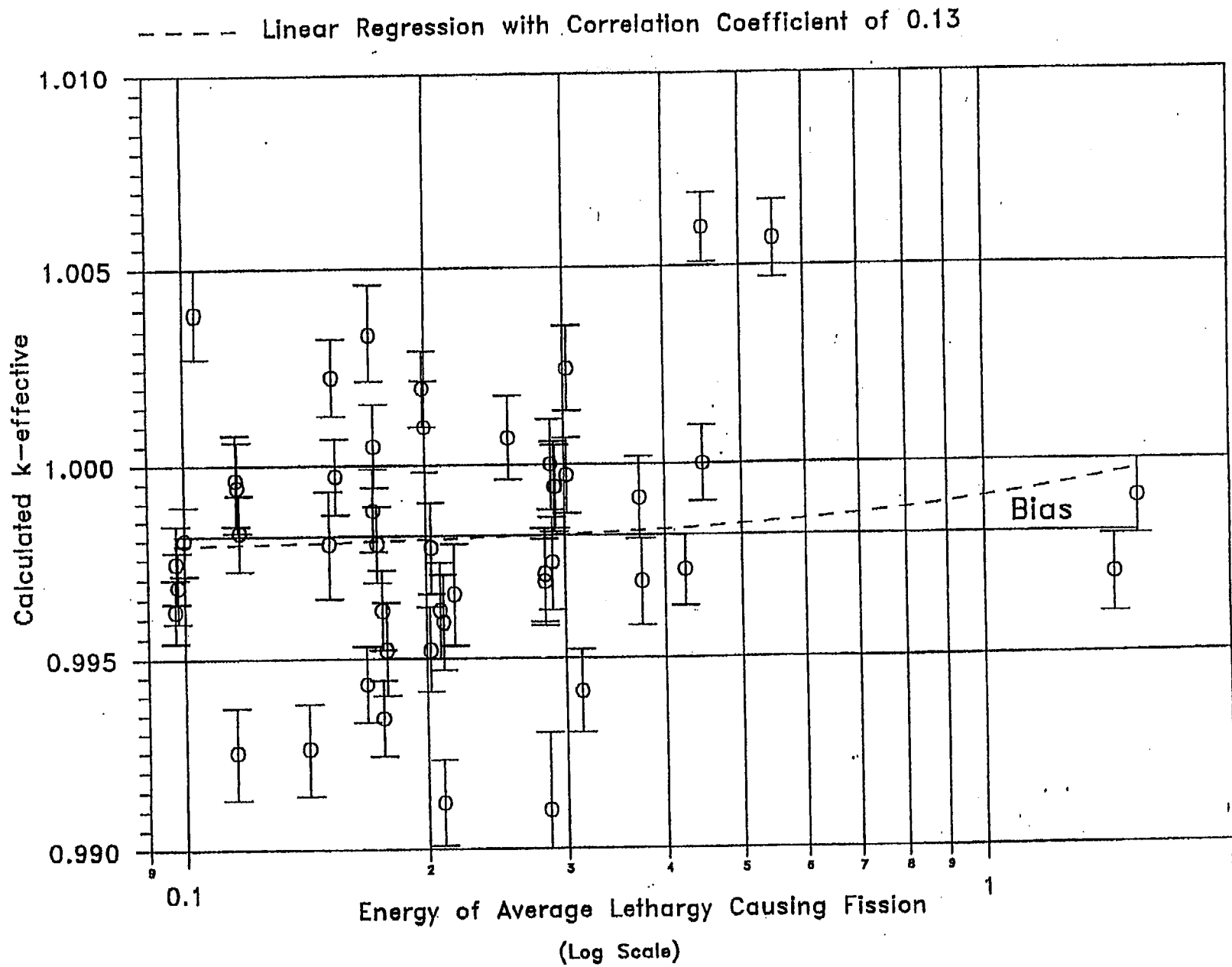


FIGURE 4A.1 MCNP CALCULATED k-eff VALUES for VARIOUS VALUES OF THE SPECTRAL INDEX

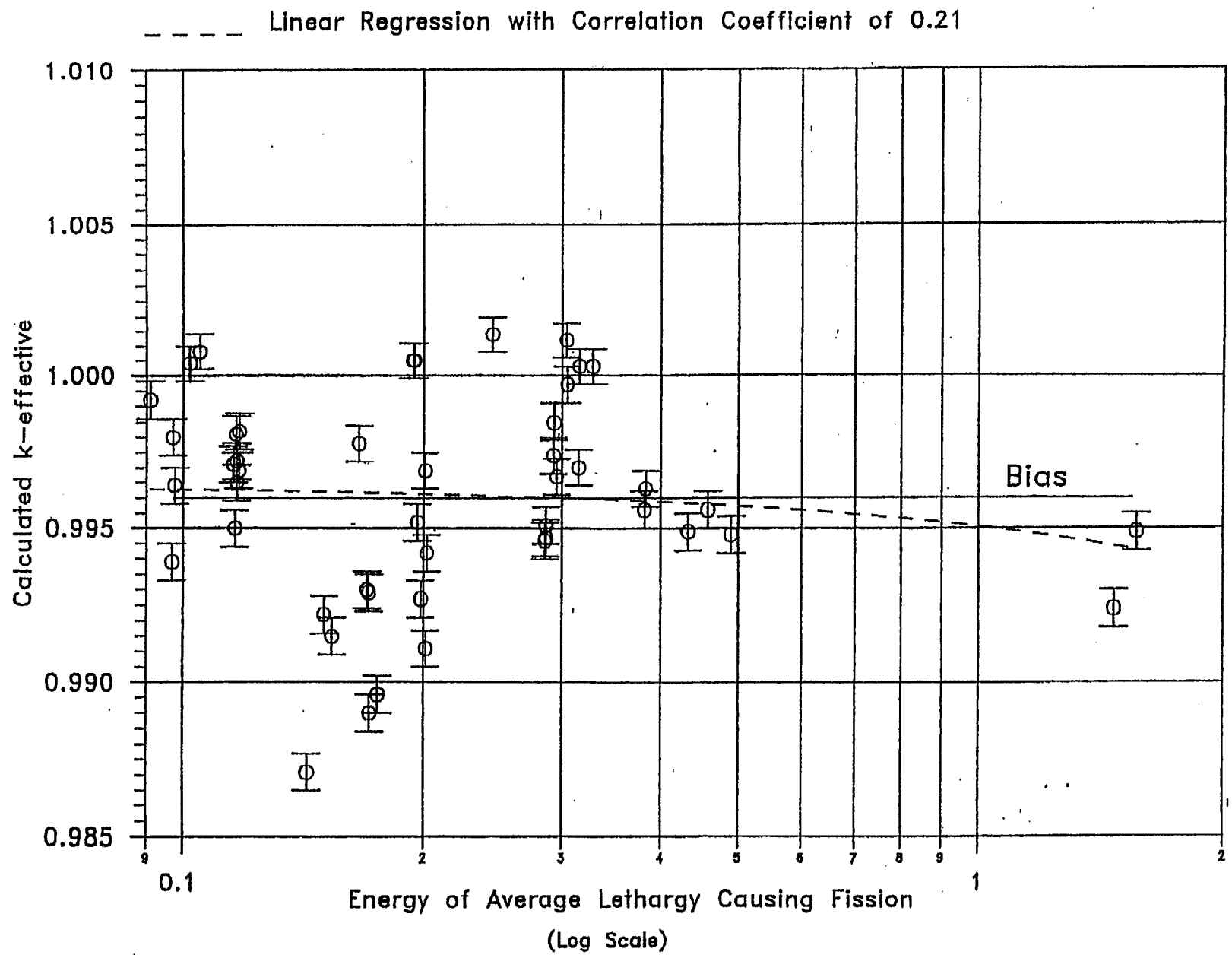


FIGURE 4A.2 KENO5a CALCULATED k -eff VALUES FOR VARIOUS VALUES OF THE SPECTRAL INDEX

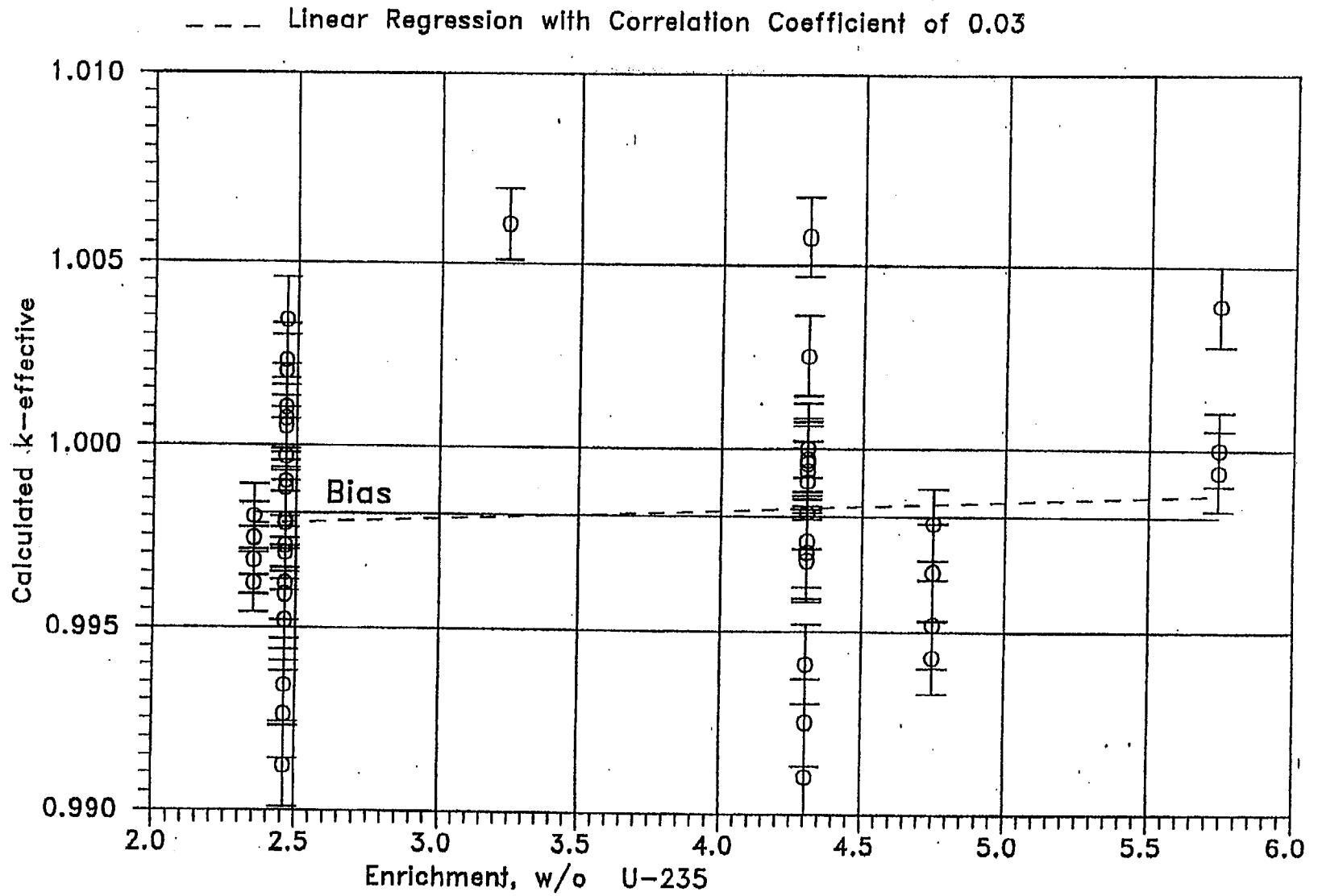


FIGURE 4A.3 MCNP CALCULATED k-eff VALUES AT VARIOUS U-235 ENRICHMENTS

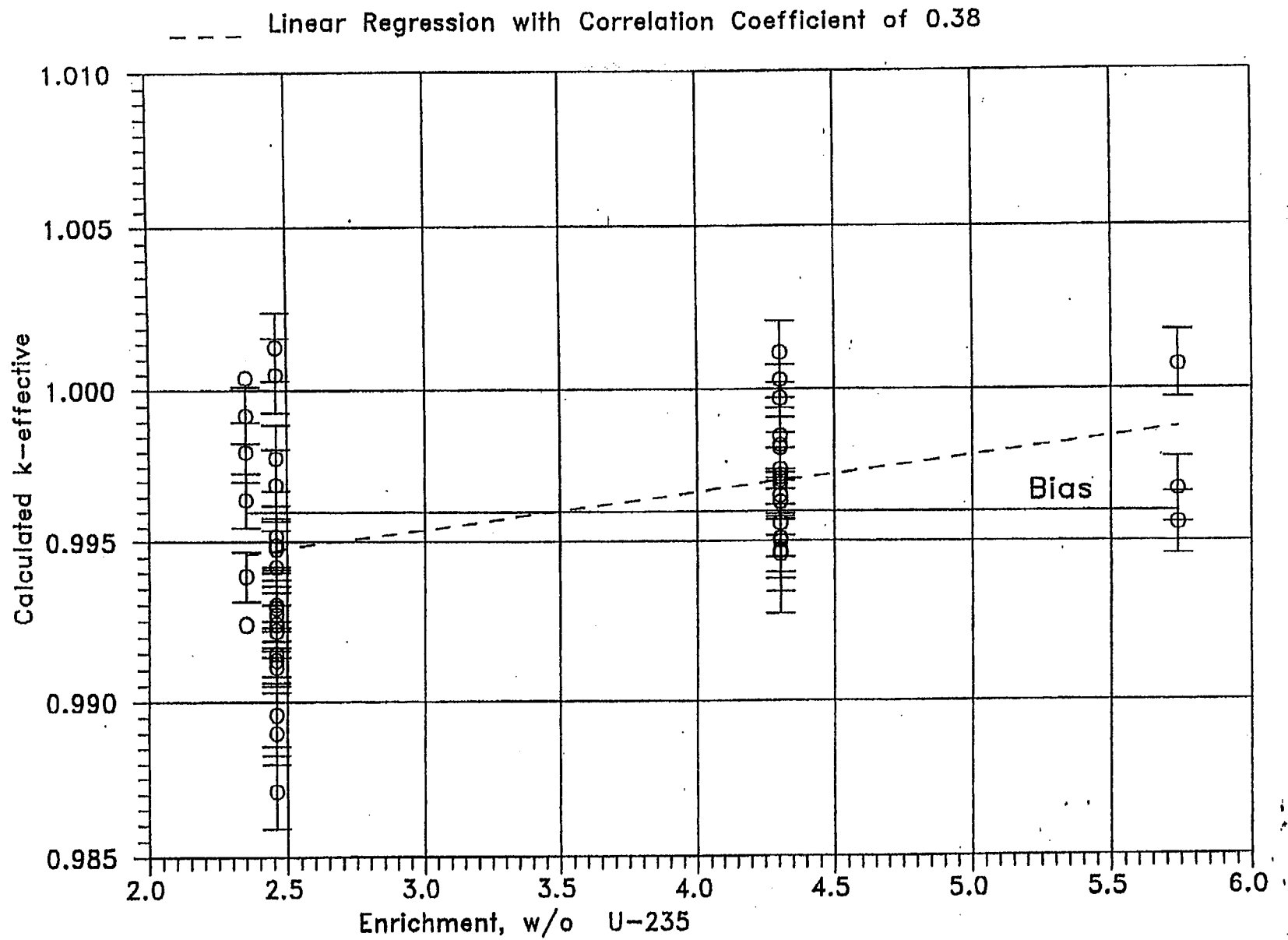


FIGURE 4A.4. KENO CALCULATED k-eff VALUES
AT VARIOUS U-235 ENRICHMENTS

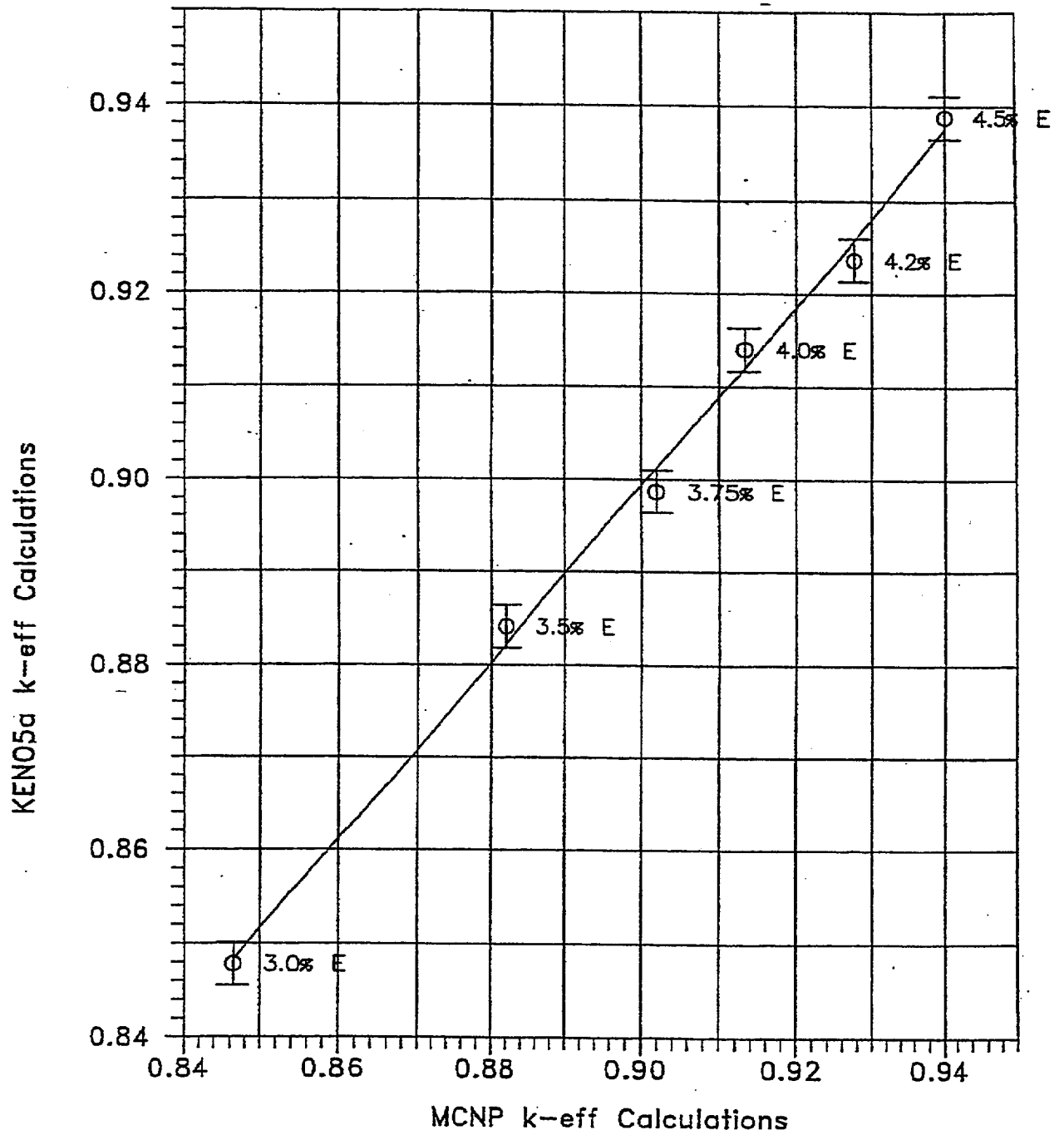


FIGURE 4A.5 COMPARISON OF MCNP AND KENO5A CALCULATIONS FOR VARIOUS FUEL ENRICHMENTS

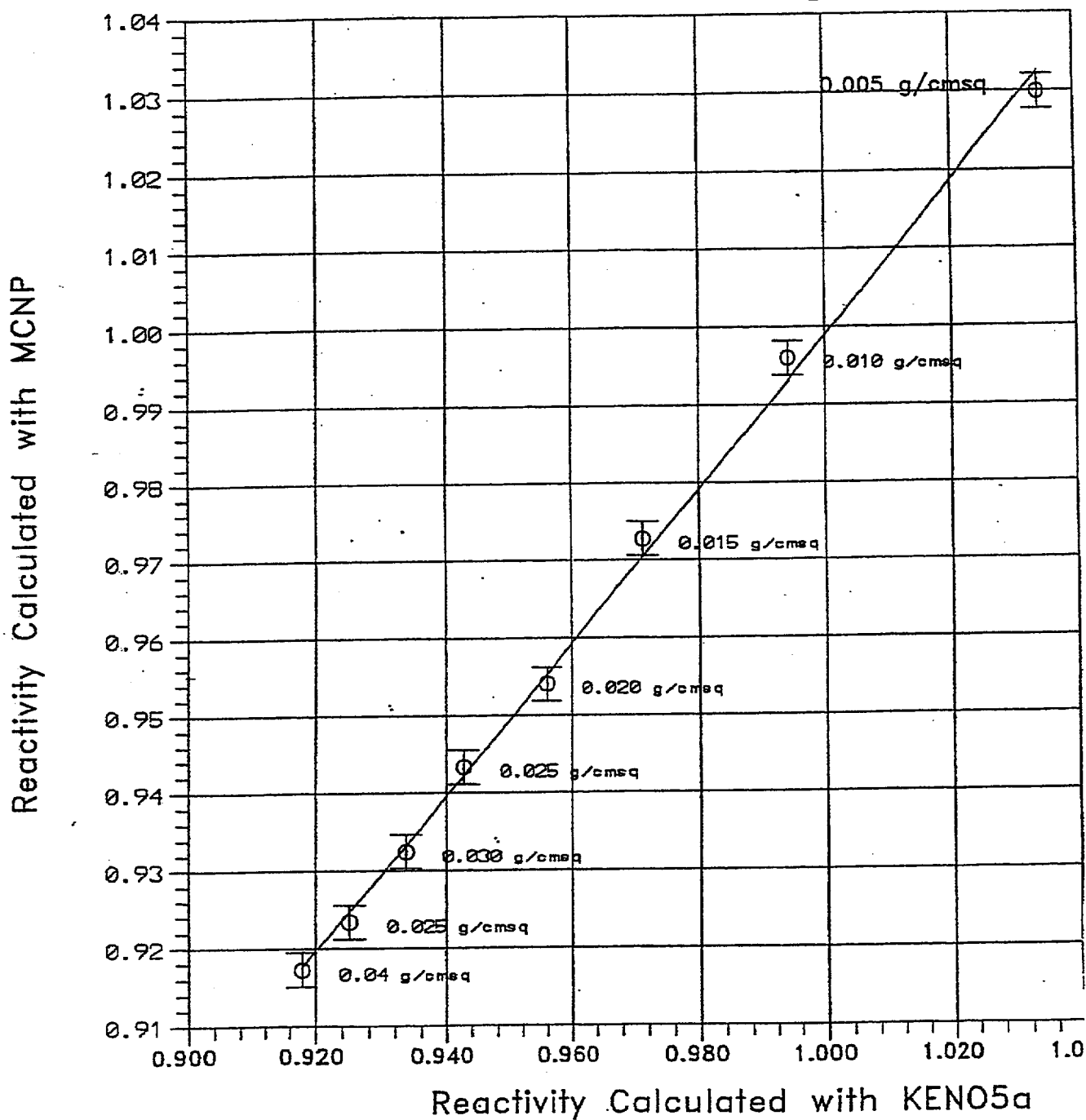


FIGURE 4A.6 COMPARISON OF MCNP AND KENO5a CALCULATIONS FOR VARIOUS BORON-10 AREAL DENSITIES

5.0 THERMAL-HYDRAULIC CONSIDERATIONS

5.1 Introduction

This document requests an operating license amendment to expand the spent fuel storage capacity at V.C. Summer. As discussed in Section 1.0, this capacity expansion would be achieved by replacing the existing spent fuel storage racks (SFSRs) with new maximum density SFSRs. This section provides a summary of the analyses performed to demonstrate the compliance of the SFP and its attendant cooling system with the provisions of USNRC Standard Review Plan (SRP) 9.1.3 (Spent Fuel Pool Cooling and Cleanup System, Rev. 1, July 1981) and Section III of the USNRC "OT Position Paper for Review and Acceptance of Spent Fuel Storage and Handling Applications," (April 14, 1978). Similar methods of thermal-hydraulic analysis have been used in the licensing evaluations for other SFP capacity expansion projects.

The thermal-hydraulic qualification analyses for the expanded rack array may be broken down into the following categories:

- i. Evaluation of the maximum bulk temperatures for the design-basis offload scenarios, to establish that maximum bulk temperature limits are not exceeded. While forced cooling is available, the bulk temperature is limited to 165°F during a partial core offload or a full core offload with two operating cooling loops, 170°F during a full core offload with one operating cooling loop or an abnormal full core offload.
- ii. Evaluation of loss-of-forced cooling scenarios, to establish minimum times to perform corrective actions and the associated makeup water requirements.
- iii. Determination of the maximum local water temperature, at the instant when the bulk temperature reaches its maximum value, to establish that localized boiling in the SFSRs is not possible while forced cooling is operating.
- iv. Evaluation of the maximum fuel rod cladding temperature, at the instant when the bulk temperature reaches its maximum value, to establish that nucleate boiling is not possible while forced cooling is operating.

The following sections present plant system descriptions, analysis methodologies and assumptions, a synopsis of the input data employed and summaries of the calculated results.

5.2 Cooling Systems Description

The Spent Fuel Pool Cooling System (SFPCS) at V.C. Summer cools the SFP by transferring decay heat through a heat exchanger to the component cooling water (CCW) system. The SFPCS has two cooling loops, each with one pump and one heat exchanger. Each cooling loop has a design SFP water flow rate of 1800 gpm. The SFPCS heat exchangers are shell and tube units with the following design performance:

Heat Transferred:	14×10 ⁶ Btu/hr
Shell Side Water Flow Rate:	890,000 lb/hr
Shell Side Water Inlet Temperature:	105°F
Shell Side Fouling Resistance:	0.0005 Btu/(hr×ft ² ×°F)
Tube Side Water Flow Rate:	890,000 lb/hr
Tube Side Water Inlet Temperature:	127°F
Tube Side Fouling Resistance:	0.0005 Btu/(hr×ft ² ×°F)

The cold shell side flow is from the CCW system and the hot tube side water is from the SFP.

As stated in the preceding paragraph, the *design* SFP water flow rate through a single SFPCS cooling loop is 1800 gpm. The maximum achievable SFP water flow rate is, however, considerably higher. Recent in-service flow testing of the SFPCS system has demonstrated that, with a single cooling loop in operation, an SFP water flow rate greater than 2400 gpm is achievable without creating pump cavitation or net positive suction head (NPSH) problems. During severe outage conditions, specifically the failure of one SFPCS cooling loop during a full core offload, the extra flow capacity of the SFPCS can provide additional heat removal capacity. This additional heat removal capacity is credited for full core offload scenarios with only one operating SFPCS cooling loop.

Normal makeup water for the SFP is obtained from the demineralized water storage tank. Emergency makeup water is obtained from the Safety Class 2a refueling water storage tank (RWST) or the Safety Class 2b reactor makeup water storage tank (RMWST). Pumps from three separate systems are available

to transfer water from these sources to the SFP: the spent fuel cooling and purification, reactor makeup water and demineralized water transfer systems.

The major components of the purification loop are the spent fuel purification pump, spent fuel cooling demineralizer, and two spent fuel purification filters in parallel. Normally the purification loop takes suction from the spent fuel pool skimmers, pumps the water through the spent fuel cooling demineralizer and the spent fuel purification filters, and returns the water to the spent fuel pool. This loop can also take suction from the spent fuel pool, RWST, cask loading area skimmer, refueling cavity, fuel transfer canal drain or cask loading area drain. The purification loop can also discharge to the RWST, fuel transfer canal, refueling cavity, and the return line to the cask loading area.

5.3 Offload/Cooling Alignment Scenarios

Three offload scenarios are postulated. These scenarios are:

Scenario	Offload Type	Number of Assemblies Offloaded
1	Partial Core	72
2	Full Core	157
3	Abnormal Full Core	72 + 157

A partial core offload is comprised of 72 assemblies offloaded into a SFP that already contains 1,709 previously offloaded assemblies. This analyzed stored fuel inventory (1,781) conservatively exceeds the maximum possible inventory of 1,712 assemblies. The decay time of the previously offloaded fuel assemblies for this scenario is assumed to be 18 months. A single loop of the SFPCS is operating (i.e. single active failure) to remove decay heat from the SFP.

A full core offload is comprised of 157 assemblies offloaded into a SFP that already contains 1,565 previously offloaded assemblies. This analyzed fuel inventory (1,722) conservatively exceeds the

maximum possible inventory of 1,712 assemblies. The 157 offloaded assemblies are separated into three distinct groups: 72 assemblies with 4.5 years of irradiation at full power, 72 assemblies with 3 years of irradiation at full power and 13 assemblies with 1.5 years of irradiation at full power. The decay time of the previously offloaded fuel assemblies for this scenario is assumed to be 18 months. Two separate cooling alignments are considered for the full core offload. The first alignment, referred to as Scenario 2a, has two SFPCS cooling loops operating to remove decay heat from the SFP. The second alignment, referred to as Scenario 2b, has only one SFPCS cooling loop operating (i.e. single active failure) but credits a higher SFP water flow rate of 2400 gpm as explained previously.

An abnormal full core offload is comprised of 157 assemblies offloaded into a SFP that already contains 1,565 previously offloaded assemblies. This analyzed fuel inventory (1,722) conservatively exceeds the maximum possible inventory of 1,712 assemblies. The 157 offloaded assemblies are separated into three distinct groups: 72 assemblies with 3 years plus 36 days of irradiation at full power, 72 assemblies with 1.5 years plus 36 days of irradiation at full power and 13 assemblies with 36 days of irradiation at full power. The decay time of the previously offloaded fuel assemblies for this scenario is assumed to be 36 days. Two SFPCS cooling loops operate to remove decay heat from the SFP.

Each of these offload/cooling scenarios is evaluated to determine the peak SFP bulk temperature. If necessary to prevent exceeding the allowable SFP bulk temperature limits, in-core hold times in excess of the normal minimum value of 72 hours are determined. Scenarios 1, 2a and 3 are each evaluated for a single, bounding maximum CCW temperature. Scenario 2b, the most limiting thermal scenario as a result of its full core offload heat load and single active failure cooling capacity, is evaluated over a range of CCW temperatures to determine CCW temperature dependent in-core hold time requirements.

Table 5.3.1 presents the historic and projected offload schedule used for these analyses.

5.4 Maximum Pool Bulk Temperatures

In this section, we present the methodology for calculating the maximum SFP bulk temperatures for the scenarios presented in the preceding section.

The following conservatisms are applied in the maximum SFP bulk temperature calculations:

- The reactor thermal power level is increased by 2% to account for the plant's reactor thermal power calorimetric uncertainty.
- Bounding parameters (i.e., burnup, batch size and initial enrichment) are used for all projected offloads. The burnup and batch size are maximized and the initial enrichment is minimized. Minimizing the initial enrichment results in a fission product spectrum that slightly increases the resulting decay heat.
- The total fuel inventories stored in the SFP are assumed to slightly exceed the 1,712 maximum storage locations.
- For a planned full-core offload, the assemblies in the core are split into three regions with burnup levels corresponding to once, twice and thrice burned. The thrice-burned and twice-burned regions are each assumed to be the size of the maximum refueling batch size, resulting in the maximum number of assemblies having the highest possible burnups.
- For an abnormal full-core offload, the assemblies in the core are split into three regions with burnup levels corresponding to 36 days at power, once-burned plus 36 days at power and twice-burned plus 36 days at power. The twice-burned plus 36 days and once-burned plus 36 days regions are each assumed to be the size of the maximum refueling batch size, resulting in the maximum number of assemblies having the highest possible burnups.
- For an abnormal full-core offload, the refueling outage immediately before the core offload is assumed to be zero days long. Thus, the two reactor shutdowns are separated by exactly 36 days and the second shutdown occurs after 36 days of operation.
- The thermal performance of the SFPCS heat exchangers is determined with all heat transfer surfaces fouled to their design-basis maximum levels.
- The thermal performance of the SFPCS heat exchangers is determined incorporating a 5% tube plugging allowance.

- The thermal inertia (thermal capacity) of the SFP is based on the net water volume only. This conservatively neglects the considerable thermal inertia of the fuel assemblies, stainless steel racks and stainless steel SFP liners.

The transient thermal response of the SFP and the attendant cooling systems is governed by a first-order, ordinary differential equation. The governing differential equation can be written by utilizing conservation of energy as:

$$C \frac{dT}{d\tau} = Q(\tau) - Q_{HX}(T) - Q_{ENV}(T) \quad (5-1)$$

where:

C = SFP thermal capacity, Btu/°F

T = SFP bulk temperature, °F

τ = Time after reactor shutdown, hr

$Q(\tau)$ = Time varying decay heat generation rate, Btu/hr

$Q_{HX}(T)$ = Temperature dependent SFPCS heat rejection rate, Btu/hr

$Q_{ENV}(T)$ = Temperature dependent passive heat loss to the environment, Btu/hr

$Q_{HX}(T)$ in Equation 5-1 is a function of the SFP bulk temperature and the coolant water flow rate and temperature, and can be written in terms of the temperature effectiveness (p) as follows:

$$Q_{HX}(T) = W_t C_t p (T - t_i) \quad (5-2)$$

where:

W_t = Coolant water flow rate, lb/hr

C_t = Coolant water specific heat capacity, Btu/(lb-°F)

p = SFPCS heat exchanger temperature effectiveness

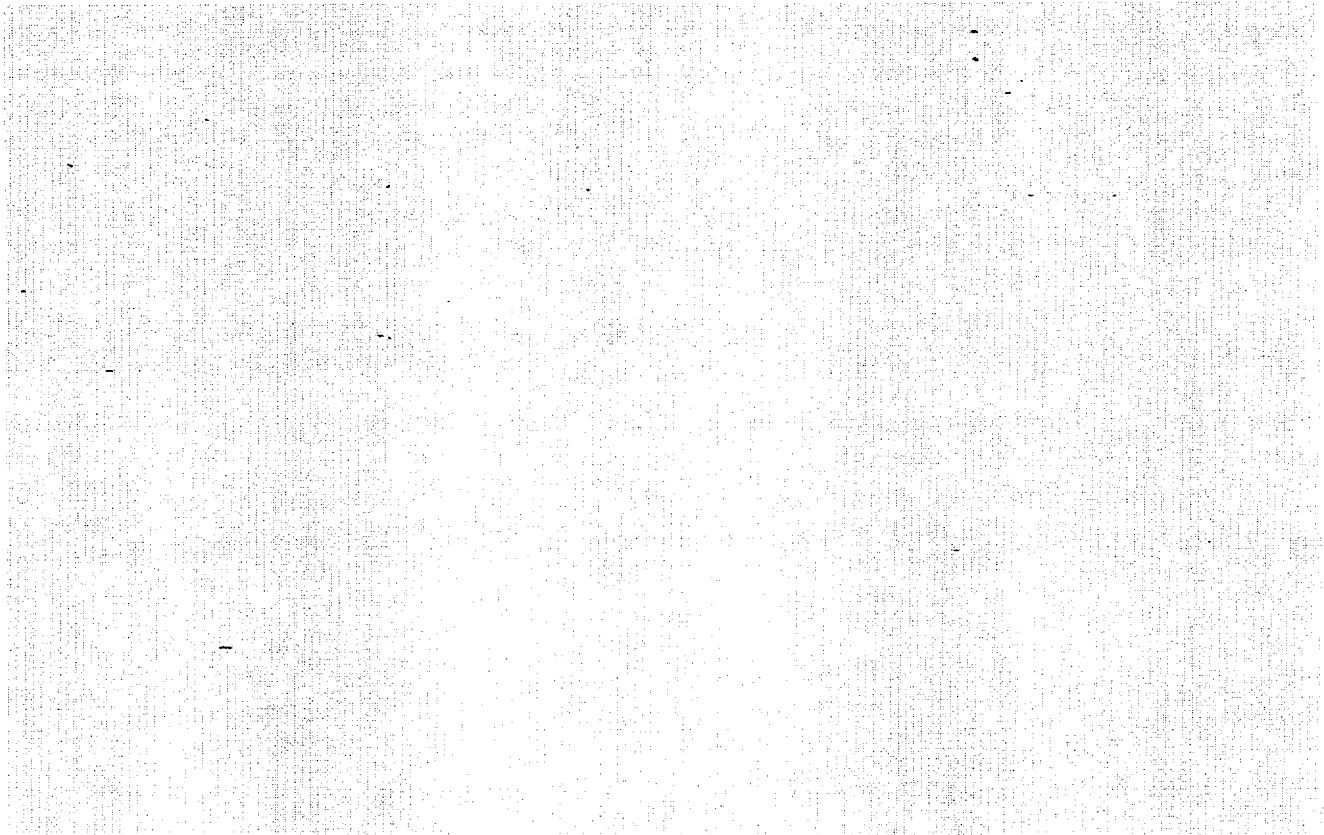
T = SFP bulk water temperature, °F

t_i = Coolant water inlet temperature, °F

The temperature effectiveness, a measure of the heat transfer efficiency of a heat exchanger, is defined as:

$$p = \frac{t_o - t_i}{T - t_i} \quad (5-3)$$

where t_o is the coolant outlet temperature ($^{\circ}\text{F}$) and all other terms are as defined above. The SFPCS heat exchanger coolant outlet temperature (t_o) for various SFP bulk temperatures (T) are determined using the Holtec QA validated computer program STER [5.4.7].



The differential equation that defines the transient thermal response of the SFP (Equation 5-1) is solved numerically. The decay heat load from previously offloaded fuel assemblies is calculated using Holtec's QA validated LONGOR computer program [5.4.3]. This program incorporates the ORIGEN2 computer code [5.4.4] to perform the decay heat calculations. The transient decay heat loads and SFP bulk temperatures are calculated using Holtec's QA validated BULKTEM computer program [5.4.5], which also incorporates the ORIGEN2 computer code. The maximum SFP bulk temperature is extracted from the results of the transient evaluations. The major input values for this analysis are summarized in Table 5.4.1.

As the SFP temperature exceeds the building ambient temperature, both heat and moisture are rejected from the surface to the SFP into the building air. Equation 5-4 utilizes the temperature of the air directly above the SFP to calculate the heat removed from the SFP by passive mechanisms. The following enthalpy and moisture balance equations govern the interaction between heat and moisture rejection at the SFP surface and absorption by the air:

$$m_{oad} h_{oad} + m_{oaw} h_{oaw} + Q_{sens} + m_{evap} h_{evap} = m_{bad} h_{bad} + m_{baw} h_{baw} \quad (5-5)$$

$$m_{oaw} + m_{evap} = m_{baw}$$

where:

- m_{oad} = Mass flow rate of incoming dry air, lb/hr
- h_{oad} = Enthalpy of incoming dry air, Btu/lb
- m_{oaw} = Mass flow rate of incoming water vapor, lb/hr
- h_{oaw} = Enthalpy of incoming water vapor, Btu/lb
- Q_{sens} = Sensible heat transferred from SFP, Btu/hr
- m_{evap} = Mass flow rate from surface of SFP, lb/hr
- h_{evap} = Enthalpy of evaporated pool water, Btu/lb
- m_{bad} = Mass flow rate of dry air above SFP, lb/hr
- h_{bad} = Enthalpy of dry air above SFP, Btu/lb
- m_{baw} = Mass flow rate of water vapor above SFP, lb/hr
- h_{baw} = Enthalpy of water vapor above SFP, Btu/lb

To determine bounding maximum values for the temperature of the air directly above the SFP, heat and moisture transfer rates from the surface of the SFP with SFP temperatures equal to the allowable bulk temperature limits are calculated using Equation 5-4. Equation 5-5 is then used to determine the enthalpies of the dry air and water vapor directly above the SFP, which are subsequently used to determine the corresponding temperature. As the SFP bulk temperatures cannot exceed the limits, this ensures bounding maximum temperatures for the air directly above the SFP for subsequent use in solving Equation 5-1.

5.5 Minimum Time-to-Boil and Maximum Boiloff Rate

In this section, we present the methodology for calculating the minimum time-to-boil and corresponding maximum boiloff rate for the scenarios presented in Section 5.3.

The following conservatisms and assumptions are applied in the time-to-boil and boiloff rate calculations:

- The thermal inertia (thermal capacity) of the SFP is based on the net water volume only. This conservatively neglects the considerable thermal inertia of the fuel assemblies, stainless steel racks and stainless steel SFP liners.
- During the loss of forced cooling evaluations, it is assumed that makeup water is not available. This minimizes the thermal capacity of the SFP as water is boiled off, thus increasing the water level drop rate.
- The loss of forced cooling is assumed to occur coincident with the peak SFP bulk temperature. Maximizing the initial temperature will conservatively minimize the calculated time-to-boil.

The governing enthalpy balance equation for this condition, subject to these conservative assumptions, can be written as:

$$C(\tau) \frac{dT}{d\tau} = Q(\tau + \tau_0) - Q_{ENV}(T) \quad (5-6)$$

where:

$C(\tau)$ = Time-varying SFP thermal capacity

τ = Time after cooling is lost (hr)

τ_0 = Loss of cooling time after shutdown (hr)

All other terms in this equation are the same as defined for Equation 5-1 in Section 5.4.

Equation 5-6 is solved using a numerical solution technique to obtain the bulk pool temperature as a function of time. The time-to-boil, boil-off rate and water depth versus time are calculated using Holtec's QA validated TBOIL program [5.4.6]. The SFP decay heat loads for these analyses are extracted from the results of the BULKTEM transient evaluations. The major input values for these analyses are summarized in Table 5.5.1.

5.6 Maximum SFP Local Water Temperature

In this section, a summary of the methodology for evaluating the maximum SFP local water temperature is presented. The results of these evaluations are maximum local water temperatures.

In order to determine an upper bound on the maximum local water temperature, a series of conservative assumptions are made. The most important of these assumptions are:

- The walls and floor of the SFP are all modeled as adiabatic surfaces, thereby neglecting conduction heat loss through these items.
- Heat losses by thermal radiation and natural convection from the hot SFP surface to the environment are neglected.
- No downcomer flow is assumed to exist between the rack modules.
- The hydraulic resistance of every SFSR cell is determined based on the most hydraulically limiting fuel assembly type, the Westinghouse 17×17 Standard.
- The hydraulic resistance parameters for the rack cells, permeability and inertial resistance, are conservatively adjusted by 10%.
- The bottom plenum heights used in the model are less than the actual heights.
- The hydraulic resistance of every SFSR cell is determined based on the most restrictive water inlet geometry of the cells over rack support pedestals (i.e., all baseplate holes are completely blocked). These cells have a reduced water entrance area, caused by the pedestal blocking the baseplate hole, and a correspondingly increased hydraulic resistance.
- The hydraulic resistance of every SFSR cell includes the effects of blockage due to an assumed dropped fuel assembly lying horizontally on top of the SFSRs.

As part of the installation of the new SFSRs, the piping that connects the SFPCS to the SFP will be modified to increase the distance between the piping and the SFSRs. It is not apparent from heuristic reasoning alone that the cooled water delivered to the SFP would not bypass the hot fuel and exit through the outlet piping. To demonstrate adequate cooling of hot fuel in the SFP, it is therefore necessary to rigorously quantify the coupled velocity and temperature fields created by the interaction of

buoyancy driven and forced water flows. A Computational Fluid Dynamics (CFD) analysis for this demonstration is required. The objective of this study is to demonstrate that the thermal-hydraulic criterion of ensuring local subcooled conditions in the SFP is met for all postulated fuel offload/cooling alignment scenarios. The local thermal-hydraulic analysis is performed such that partial cell blockage and slight fuel assembly variations are bounded. An outline of the CFD approach is described in the following.

There are several significant geometric and thermal-hydraulic features of the V.C. Summer SFP that need to be considered for a rigorous CFD analysis. From a fluid flow modeling standpoint, there are two regions to be considered. One region is the SFP bulk region where the classical Navier-Stokes equations [5.6.1] are solved, with turbulence effects included. The other region is the SFSRs containing heat generating fuel assemblies, located near the bottom of the SFP. In this region, water flow is directed vertically upwards due to buoyancy forces through relatively small flow channels formed by the hydraulically most resistive Westinghouse 17×17 Standard fuel assemblies in each SFSR cell. This situation is modeled as a porous solid region with pressure drop in the flowing fluid governed by Darcy's Law as:

$$\frac{\partial P}{\partial X_i} = -\frac{\mu}{K(i)} V_i - C \rho |V| \frac{V_i}{2} \quad (5-7)$$

where $\partial P/\partial X_i$ is the pressure gradient, $K(i)$, V_i and C are the corresponding permeability, velocity and inertial resistance parameters and μ is the fluid viscosity. These terms are added to the classic Navier-Stokes equations. The permeability and inertial resistance parameters for the rack cells loaded with Westinghouse 17×17 Standard fuel assemblies are determined based on friction factor correlations for the laminar flow conditions that would exist due to the low buoyancy induced velocities and the small size of the flow channels.

The V.C. Summer SFP geometry requires an adequate portrayal of both large scale and small scale features, spatially distributed heat sources in the SFSRs and water inlet/outlet piping. Relatively cooler

bulk water normally flows down between the fuel racks outline and wall liner, a clearance known as the downcomer. Near the bottom of the racks the flow turns from a vertical to horizontal direction into the bottom plenum, supplying cooling water to the rack cells. Heated water issuing out of the top of the racks mixes with the bulk water. An adequate modeling of these features on the CFD program involves meshing the large scale bulk SFP region and small scale downcomer and bottom plenum regions with sufficient number of computational cells to capture both the global and local features of the flow field.

The distributed heat sources in the spent fuel pool racks are modeled by identifying distinct heat generation zones considering recently offloaded fuel, bounding peaking effects, and the presence of background decay heat from previous offloads. Three heat generating zones are modeled. The first consists of background fuel from previous offloads. The second and third zones consist of fuel from recently offloaded fuel assemblies. The two recent offload zones are differentiated by one zone with higher than average decay (hottest partial core offload batch) heat generation and the other with less than average decay heat generation (remainder of full core). This is a conservative model, since all of the fuel with higher than average decay heat is placed in a contiguous area. A uniformly distributed heat generation rate was applied throughout each distinct zone (i.e., there were no variations in heat generation rate within a single zone).

The CFD analysis was performed on the commercially available FLUENT [5.6.2] computational fluid dynamics program, which has been benchmarked under Holtec's QA program. The FLUENT code enables buoyancy flow and turbulence effects to be included in the CFD analysis. Buoyancy forces are included by specifying a temperature-dependent density for water and applying an appropriate gravity vector. Turbulence effects are modeled by relating time-varying Reynolds' Stresses to the mean bulk flow quantities with the standard k- ϵ turbulence model.

Some of the major input values for this analysis are summarized in Table 5.6.1. An isometric view of the assembled CFD model for the V.C. Summer SFP is presented in Figure 5.6.1.

5.7 Fuel Rod Cladding Temperature

In this section, the method to calculate the temperature of the fuel rod cladding is presented. As previously stated in Section 5.1, the maximum fuel rod cladding temperature is determined to establish that nucleate boiling is not possible while forced cooling is operating. This requires demonstrating that the highest fuel rod cladding temperatures are less than the local saturation temperature of the adjacent SFP water. The maximum fuel cladding superheat above the local water temperature is calculated for two different peak fuel rod heat emission rates.

A fuel rod can produce F_z times the average heat emission rate over a small length, where F_z is the axial peaking factor. The axial heat distribution in a rod is generally a maximum in the central region, and tapers off at its two extremities. Thus, peak cladding heat flux over an infinitesimal rod section is given by the equation:

$$q_c = \frac{Q \times F_z}{A_c} \quad (5-8)$$

where Q is the rod average heat emission and A_c is the total cladding external heat transfer area in the active fuel length region. The axial peaking factor is given in Table 5.6.1.

As described previously, the maximum local water temperature was computed. Within each fuel assembly sub-channel, water is continuously heated by the cladding as it moves axially upwards under laminar flow conditions. Rohsenow and Hartnett [5.7.1] report a Nusselt-number for laminar flow heat transfer in a heated channel. The film temperature driving force (ΔT_f) at the peak cladding flux location is calculated as follows:

$$\Delta T_f = \frac{q_c}{h_f} \quad (5-9)$$
$$h_f = \text{Nu} \frac{K_w}{D_h}$$

where h_f is the waterside film heat transfer coefficient, D_h is sub-channel hydraulic diameter, K_w is water thermal conductivity and Nu is the Nusselt number for laminar flow heat transfer.

In order to introduce some additional conservatism in the analysis, we assume that the fuel cladding has a crud deposit resistance R_c (equal to $0.0005 \text{ ft}^2\text{-hr-}^\circ\text{F/Btu}$) which covers the entire surface. Thus, including the temperature drop across the crud resistance, the cladding to water local temperature difference (ΔT_c) is given by the equation $\Delta T_c = \Delta T_f + R_c \times q_c$.

5.8 Results

This section contains results from the analyses performed for the postulated offload scenarios.

5.8.1 Maximum Pool Bulk Temperatures

For the offload/cooling scenarios described in Section 5.3, the maximum calculated bulk temperatures and corresponding in-core hold time requirements are summarized in Table 5.8.1. The results presented in Table 5.8.1 demonstrate that all calculated bulk temperatures remain below the allowable limits, with the identified in-core hold times. Given the conservatisms incorporated into the calculations, actual bulk temperatures will be lower than these calculated values.

Figures 5.8.1 through 5.8.7 each present profiles of net decay heat load, passive heat losses and bulk temperature versus time for the evaluated transient scenarios. A plot of the required in-core hold time as a function of CCW temperature for Scenario 2b is presented in Figure 5.8.8. Calculated decay heat loads for each offload batch of the most limiting offload scenario, the full core offload with one operating cooling loop, are summarized in Table 5.8.4. Note that the reported decay heat loads for the end-of-cycle 24 fuel assemblies are coincident with the calculated peak bulk temperature.

5.8.2 Minimum Time-to-Boil and Maximum Boiloff Rate

For the offload/cooling described in Section 5.3, the calculated times-to-boil and maximum boil-off rates are summarized in Table 5.8.2. These results show that, in the extremely unlikely event of a failure of forced cooling to the SFP, there would be at least 2.07 hours available for corrective actions prior to SFP boiling. Given the conservatisms incorporated into the calculations, actual times-to-boil will be higher than these calculated values. It is noted that a complete failure of forced cooling is extremely unlikely because there are two SFPCS cooling loops powered from independent safeguards trains.

The maximum water boiloff rate is less than 91 gpm. This is less than the makeup capacity available from the RWST or RMWST.

5.8.3 Local Water and Fuel Cladding Temperatures

Consistent with our approach to make conservative assessments of temperature, the local water temperature calculations are performed for an SFP with a total decay heat generation equal to the calculated decay heat load coincident with the maximum SFP bulk temperature. Thus, the local water temperature evaluation is a calculation of the temperature increment over the theoretical spatially uniform value due to local hot spots (due to the presence of highly heat emissive fuel assemblies). As described in Subsection 5.7, the peak fuel clad superheats (i.e., the maximum clad-to-local water temperature difference) are determined for two peak fuel rod heat emission levels. The resultant bounding superheat values were used to calculate bounding maximum fuel clad temperatures.

The numeric results of the maximum local water temperature and the bounding fuel cladding temperature evaluations are presented in Table 5.8.3. Figure 5.8.9 presents converged temperature contours in a vertical slice through the hot fuel region. Figure 5.8.10 presents converged velocity vectors in a vertical slice through the hot fuel region.

Both the maximum local water temperatures and the bounding fuel cladding temperatures are substantially lower than the 240°F local boiling temperature at the top of the SFSRs. These results demonstrate that boiling, including nucleate boiling on clad surfaces, cannot occur anywhere within the V.C. Summer SFP.

5.9 References

- [5.4.1] "Heat Loss to the Ambient from Spent Fuel Pools: Correlation of Theory with Experiment", Holtec Report HI-90477, Rev. 0, April 3, 1990.
- [5.4.2] "An Improved Correlation for Evaporation from Spent Fuel Pools", Holtec Report HI-971664, Rev. 0.
- [5.4.3] "QA Documentation for LONGOR," Holtec Report HI-951390, Revision 0.
- [5.4.4] A.G. Croff, "ORIGEN2 - A Revised and Updated Version of the Oak Ridge Isotope Generation and Depletion Code," ORNL-5621, Oak Ridge National Laboratory, 1980.
- [5.4.5] "QA Documentation for BULKTEM," Holtec Report HI-951391, Revision 1.
- [5.4.6] "QA Documentation for TBOIL," Holtec Report HI-92832, Revision 5.
- [5.4.7] "QA Documentation for STER", Holtec Report HI-92776, Revision 11.
- [5.6.1] Batchelor, G.K., "An Introduction to Fluid Dynamics", Cambridge University Press, 1967.
- [5.6.2] "Validation of FLUENT Version 5.1", Holtec Report HI-992276, Revision 0.
- [5.7.1] Rohsenow, N.M., and Hartnett, J.P., "Handbook of Heat Transfer", McGraw Hill Book Company, New York, 1973.

Table 5.3.1					
Historic and Projected Fuel Offload Schedule					
End-of-Cycle Number	Offload Date	Number of Assemblies	Average Burnup (MWd/MTU)	Initial ²³⁵U Enrichment (wt. %)	Assembly ²³⁵U Weight (kgU)
1	9/28/1984	44	17600	2.11	457.88
2	10/05/1985	9	21391	2.11	456.92
2	10/05/1985	47	27659	2.61	457.62
2	10/05/1985	10	25767	3.11	460.35
3	3/06/1987	5	29000	2.61	457.04
3	3/06/1987	40	34000	3.11	460.81
3	3/06/1987	15	30000	3.44	461.99
4	9/16/1988	21	39901	3.44	461.46
4	9/16/1988	36	37000	3.84	460.15
4	9/16/1988	4	45614	3.45	424.08
5	3/23/1990	1	38000	3.11	461.88
5	3/23/1990	4	31000	3.44	461.42
5	3/23/1990	36	37000	3.84	460.88
5	3/23/1990	28	34000	3.60	464.57
6	9/20/1991	1	41000	3.10	462.00
6	9/20/1991	4	46000	3.80	461.00
6	9/20/1991	28	37571	3.60	464.00
6	9/20/1991	39	36846	3.83	423.08
7	3/06/1993	25	46800	4.20	424.00
7	3/06/1993	23	33739	3.80	426.00
7	3/06/1993	20	40000	4.20	425.00
8	9/09/1994	4	42747	3.80	423.00
8	9/09/1994	13	37873	3.80	426.00
8	9/09/1994	4	45453	4.20	425.00
8	9/09/1994	8	43921	3.80	415.00
8	9/09/1994	35	41315	4.20	418.06

Table 5.3.1 (continued)					
Historic and Projected Fuel Offload Schedule					
End-of-Cycle Number	Offload Date	Number of Assemblies	Average Burnup (MWd/MTU)	Initial ²³⁵U Enrichment (wt.%)	Assembly ²³⁵U Weight (kgU)
9	4/14/1996	21	40617	3.80	415.35
9	4/14/1996	1	55945	4.20	416.08
9	4/14/1996	19	41019	3.80	417.13
9	4/14/1996	27	43853	4.20	416.38
10	10/03/1997	3	45748	3.80	415.35
10	10/03/1997	12	45805	3.80	417.84
10	10/03/1997	9	48120	4.20	417.00
10	10/03/1997	40	47385	4.60	417.54
11	4/03/1999	1	57531	3.80	415.75
11	4/03/1999	24	50499	4.60	417.51
11	4/03/1999	40	50079	4.60	416.58
12	10/03/2000	72	55000	4.00	417.0
13	04/03/2002	72	55000	4.00	417.0
14	10/03/2003	72	55000	4.00	417.0
15	04/03/2005	72	55000	4.00	417.0
16	10/03/2006	72	55000	4.00	417.0
17	04/03/2008	72	55000	4.00	417.0
18	10/03/2009	72	55000	4.00	417.0
19	04/03/2011	72	55000	4.00	417.0
20	10/03/2012	72	55000	4.00	417.0
21	04/03/2014	72	55000	4.00	417.0
22	10/03/2015	72	55000	4.00	417.0
23	04/03/2017	72	55000	4.00	417.0
24	10/03/2018	72	55000	4.00	417.0
25	04/03/2020	72	55000	4.00	417.0
26	10/03/2021	72	55000	4.00	417.0

TABLE 5.4.1	
Key Input Data for Bulk Temperature Evaluation	
Number of Storage Cells in SFP	1,712
Maximum Refueling Batch Size	72 assemblies
Reactor Thermal Power 1984 through 1996 1997 through EOL	2,775 MW(t) 2,900 MW(t)
Reactor Thermal Power Uncertainty	2%
Reactor Core Size	157 assemblies
Bounding Maximum Inlet CCW Temperature	105°F
SFPCS HX Coolant Flow Rate	890,000 lb/hr
SFP Water Flow to Each SFPCS HX Partial Core - One Cooling Train Full Core - Two Cooling Trains Full Core - One Cooling Train	1800 gpm 1800 gpm 2400 gpm
Normal Minimum In-Core Hold Time	72 hrs
Minimum Fuel Assembly Transfer Time	20 hrs
Region Average Fuel Assembly Offload Burnups Once-Burned Region Twice-Burned Region Thrice-Burned Region	30,250 MWd/MTU 52,250 MWd/MTU 55,000 MWd/MTU

Table 5.5.1	
Key Input Data for Time-To-Boil Evaluation	
SFP Surface Area	1075 ft ²
Minimum Pool Water Depth	37.5 feet
Fuel Racks Displaced Volume	548 ft ³
Fuel Assemblies Displaced Volume	6,768 ft ³
SFP Net Water Volume	32,988 ft ³

Table 5.6.1	
Key Input Data for Local Temperature Evaluation	
Axial Peaking Factor	1.588
Number of Fuel Assemblies	1,712
Cooled SFP Water Flow Rate through SFPCS Heat Exchanger	2400 gpm
Hydraulically Limiting Fuel Assembly	Westinghouse 17×17 Std.
Fuel Rod Outer Diameter	0.374 inches
Active Fuel Length	144 inches
Number of Rods per Assembly	264 rods
Rack Cell Inner Dimension	8.85 inches
Rack Cell Length	167 inches
Modeled Bottom Plenum Height	4.25 inches

Scenario	Maximum Bulk Temperature (°F)	Time After Reactor Shutdown (hrs)	Coincident Net Heat Load (Btu/hr)	In-Core Hold Time (hrs)
1 - Partial Core	152.53	103	20.71×10^6	72
2a - Full Core	150.97	97	40.16×10^6	72
2b - Full Core 105°F CCW	169.90	177	31.16×10^6	146
2b - Full Core 95°F CCW	169.57	124	35.79×10^6	94
2b - Full Core 90°F CCW	169.75	104	38.22×10^6	74
2b - Full Core 85°F CCW	169.88	87	40.74×10^6	58
3 - Abnormal Full Core	149.53	97*	38.84×10^6	72

* The coincident time after reactor shutdown for the abnormal full-core offload scenario is measured from the abnormal reactor shutdown. If measured from the previous (36 days prior) shutdown, this value would be $864 + 97 = 961$ hours.

Table 5.8.2		
Results of Loss-of-Forced Cooling Evaluations		
Scenario	Minimum Time-to-Boil	Maximum Boil-Off Rate
1 - Partial Core	6.00 hrs	45.75 gpm
2a - Full Core	3.11 hrs	87.21 gpm
2b - Full Core w/105°F CCW	2.71 hrs	70.07 gpm
2b - Full Core w/95°F CCW	2.39 hrs	79.63 gpm
2b - Full Core w/90°F CCW	2.21 hrs	84.91 gpm
2b - Full Core w/85°F CCW	2.07 hrs	90.67 gpm
3 - Abnormal Full Core	3.29 hrs	84.52 gpm

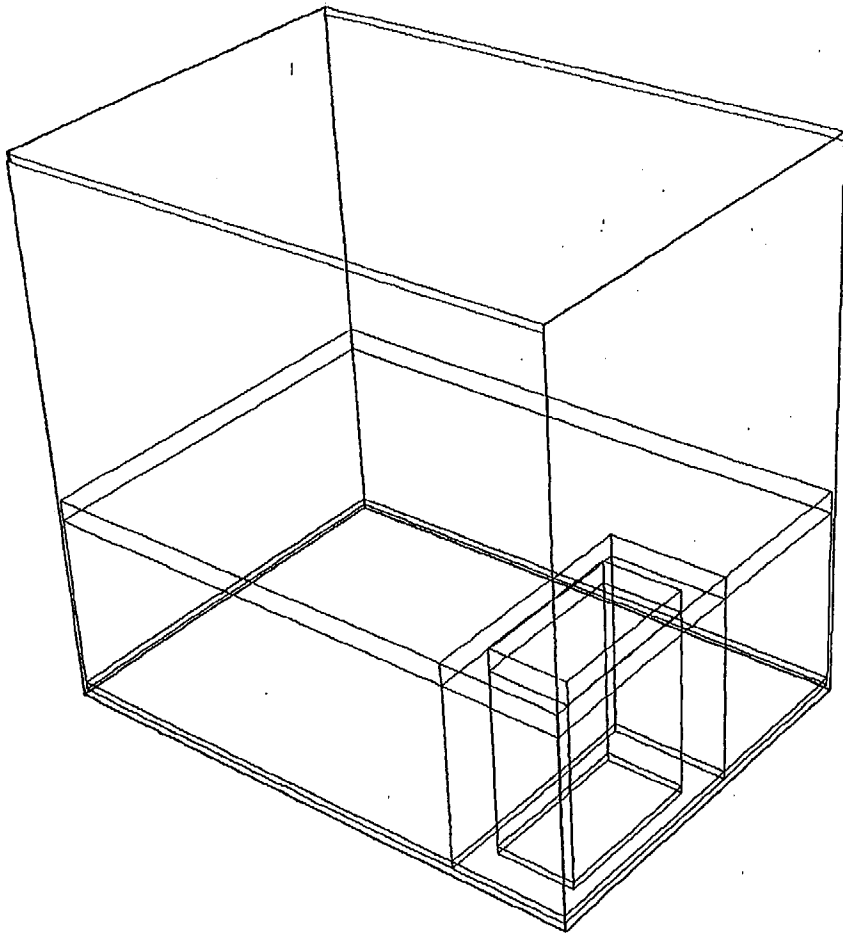
Note: For scenario 2b, the required in-core hold time is varied as a function of CCW temperature. Because SFP decay heat load varies with hold time, the time-to-boil and boil-off rate also vary.

Table 5.8.3			
Results of Maximum Local Water and Fuel Cladding Temperature Evaluations			
Peak Rod Exposure (MWd/MTU)	Maximum Local Water Temp. (°F)	Bounding Fuel Clad Superheat (°F)	Bounding Fuel Clad Temperature (°F)
62,000 -	192.7	35.8	228.5
75,000		37.7	230.4

Table 5.8.4**Calculated Batch Decay Heat Loads for Scenario 2b with 85°F CCW**

End-of-Cycle Number	Offload Date	Number of Assemblies	Avg. Burnup (MWd/MTU)	Decay Heat Load (Btu/hr)
1	9/28/1984	44	17600	28982.66
2	10/05/1985	9	21391	6910.94
2	10/05/1985	47	27659	45710.72
2	10/05/1985	10	25767	8688.60
3	3/06/1987	5	29000	5238.85
3	3/06/1987	40	34000	47905.80
3	3/06/1987	15	30000	15382.99
4	9/16/1988	21	39901	30329.06
4	9/16/1988	36	37000	46767.99
4	9/16/1988	4	45614	6223.76
5	3/23/1990	1	38000	1433.89
5	3/23/1990	4	31000	4461.80
5	3/23/1990	36	37000	48054.02
5	3/23/1990	28	34000	34633.45
6	9/20/1991	1	41000	1602.03
6	9/20/1991	4	46000	7073.98
6	9/20/1991	28	37571	39725.73
6	9/20/1991	39	36846	48841.92
7	3/06/1993	25	46800	41821.54
7	3/06/1993	23	33739	26963.14
7	3/06/1993	20	40000	27908.10
8	9/09/1994	4	42747	6271.43
8	9/09/1994	13	37873	17838.95
8	9/09/1994	4	45453	6660.81
8	9/09/1994	8	43921	12713.56
8	9/09/1994	35	41315	51237.78

Table 5.8.4 (continued)				
Calculated Batch Decay Heat Loads for Scenario 2b with 85°F CCW				
End-of-Cycle Number	Offload Date	Number of Assemblies	Avg. Burnup (MWd/MTU)	Decay Heat Load (Btu/hr)
9	4/14/1996	21	40617	31406.70
9	4/14/1996	1	55945	2189.76
9	4/14/1996	19	41019	28861.96
9	4/14/1996	27	43853	43473.02
10	10/03/1997	3	45748	5320.21
10	10/03/1997	12	45805	21442.66
10	10/03/1997	9	48120	16728.54
10	10/03/1997	40	47385	71709.23
11	4/03/1999	1	57531	2486.01
11	4/03/1999	24	50499	47981.31
11	4/03/1999	40	50079	78937.65
12	10/03/2000	72	55000	172050.30
13	04/03/2002	72	55000	178096.20
14	10/03/2003	72	55000	184859.30
15	04/03/2005	72	55000	192544.70
16	10/03/2006	72	55000	201664.70
17	04/03/2008	72	55000	213346.50
18	10/03/2009	72	55000	229229.70
19	04/03/2011	72	55000	253310.60
20	10/03/2012	72	55000	295426.50
21	04/03/2014	72	55000	381502.90
22	10/03/2015	72	55000	589623.40
23	04/03/2017	72	55000	1192773.00
24	10/03/2018	72	55000	17324091.36
		72	52250	17145008.64
		13	30250	2798627.65

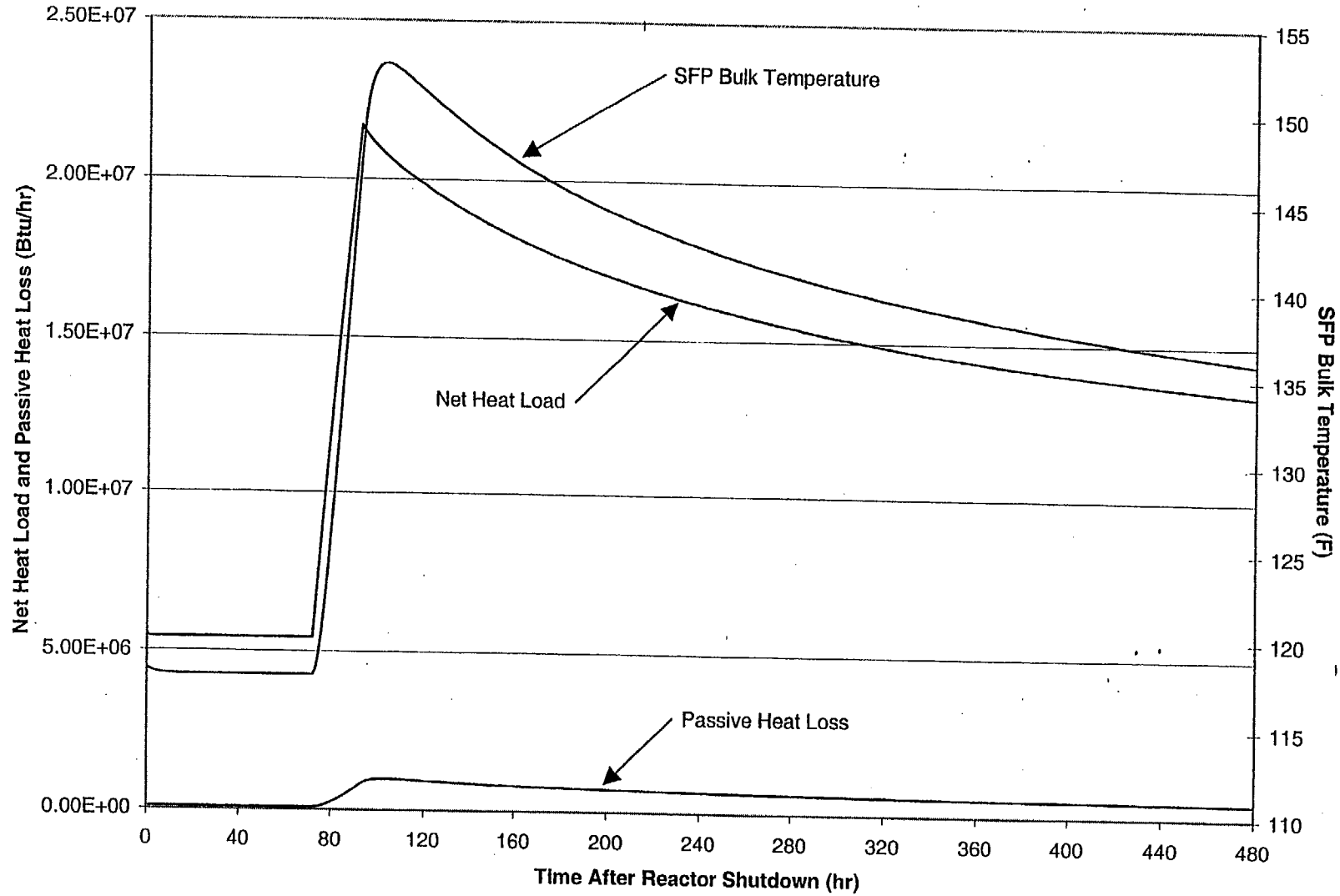


Grid
Mar 20, 2001
FLUENT 5.1 (3d, segregated, ke)

Figure 5.6.1 - Isometric View of Three-Dimensional CFD Model of the V.C. Summer SFP

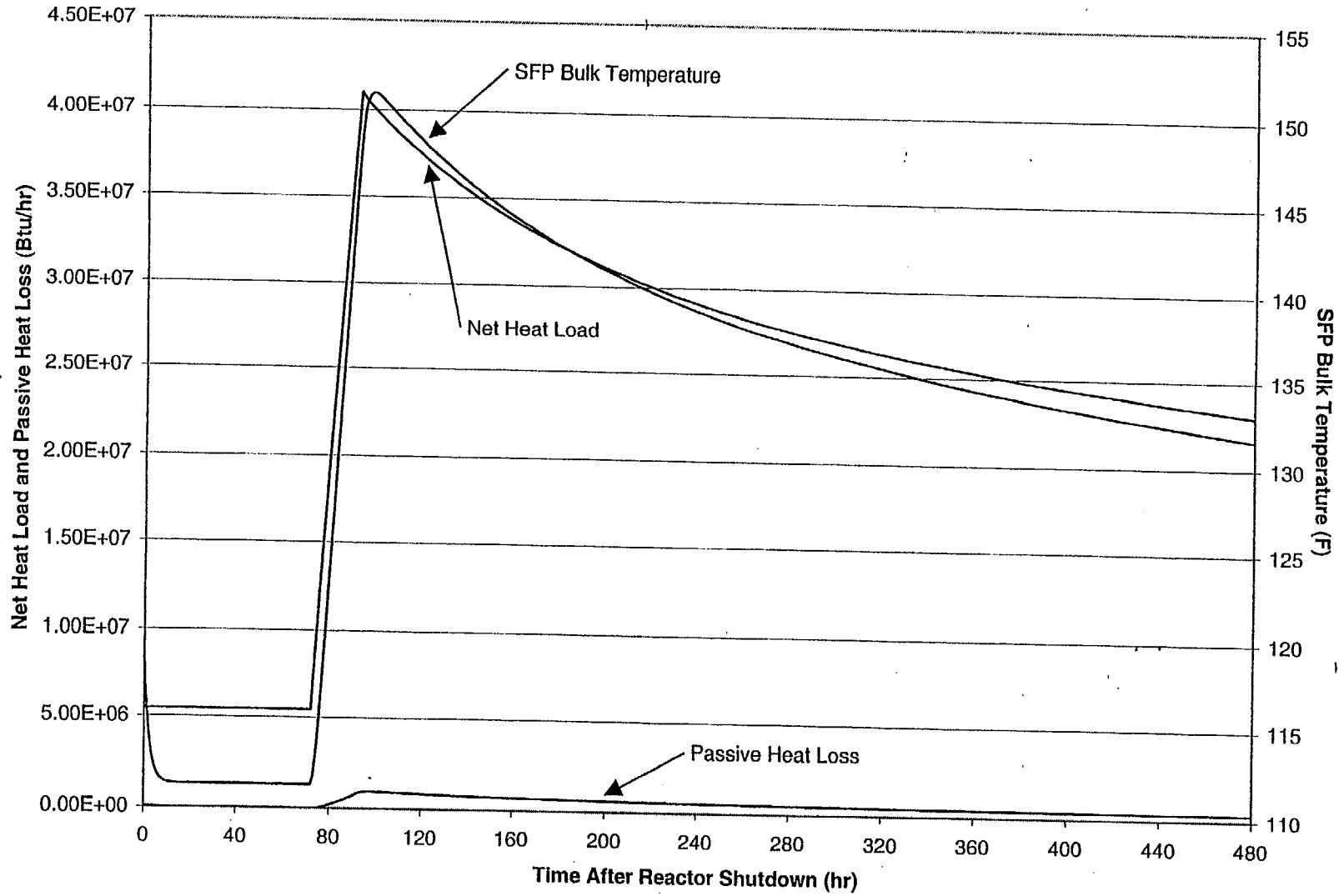
SHADED TEXT CONTAINS PROPRIETARY INFORMATION

Figure 5.8.1 - Scenario 1 Partial Core Offload
Net Heat Load, Passive Heat Loss and Bulk Temperature Profiles



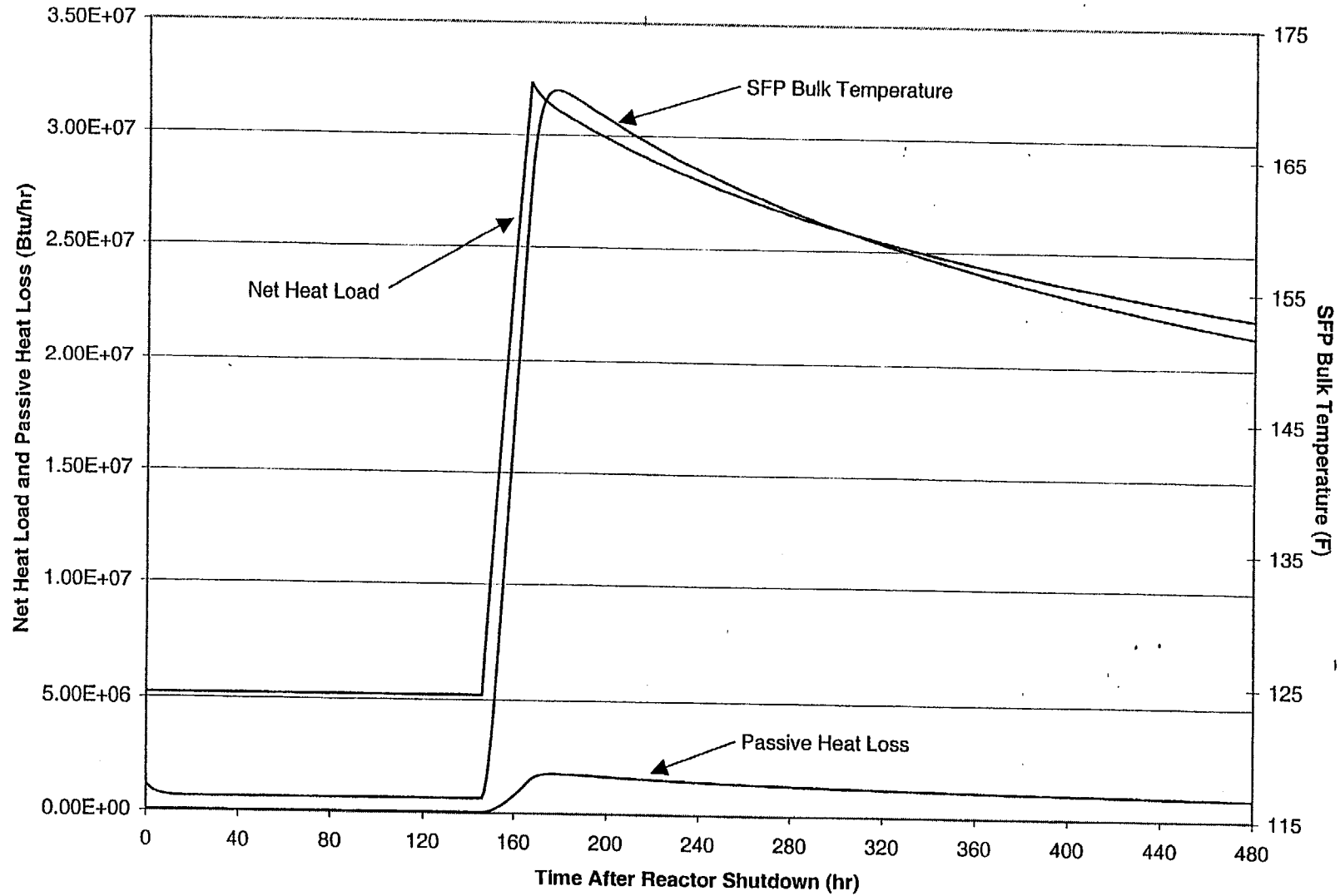
SHADED TEXT CONTAINS PROPRIETARY INFORMATION

Figure 5.8.2 - Scenario 2a Full Core Offload
Net Heat Load, Passive Heat Loss and Bulk Temperature Profiles



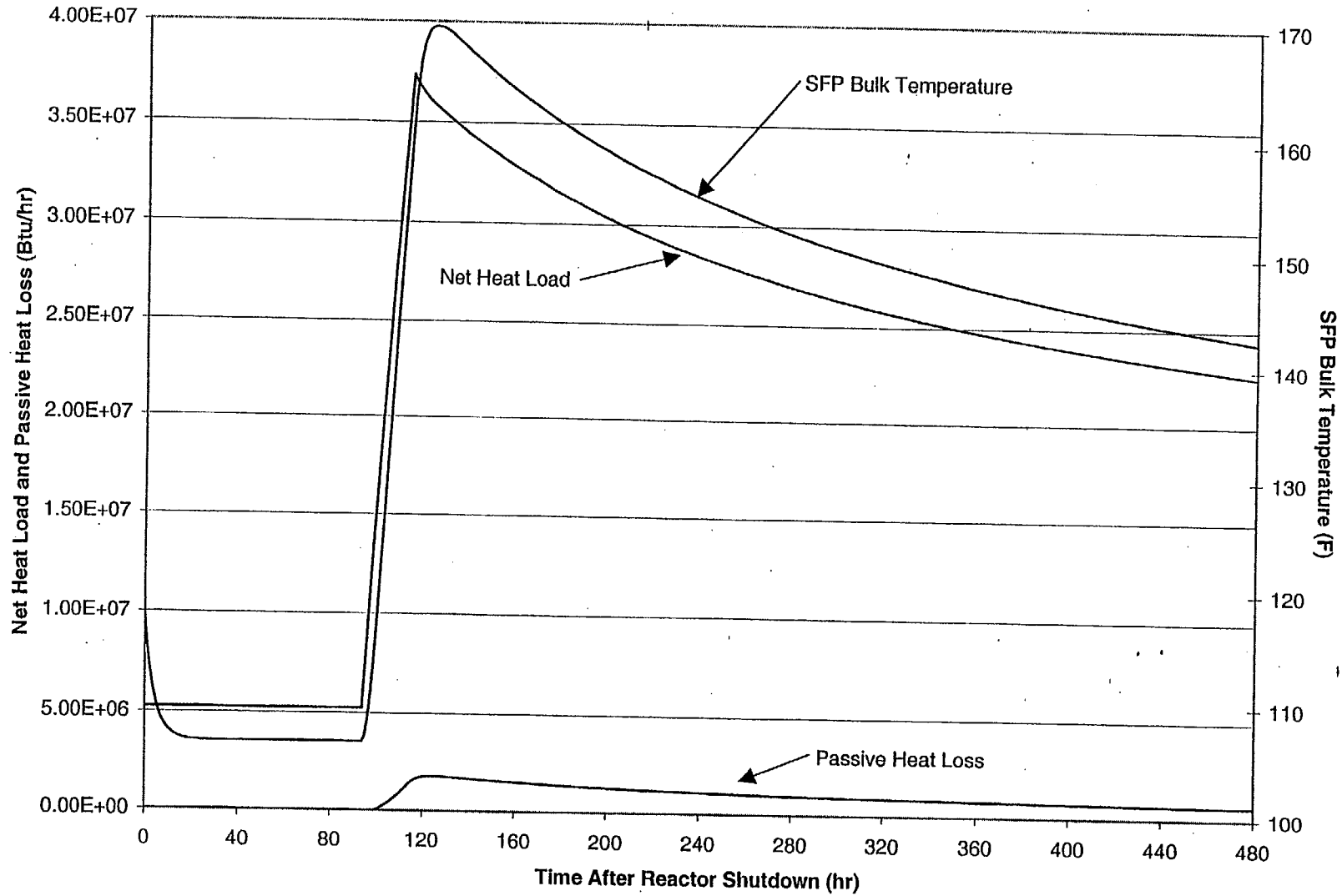
SHADED TEXT CONTAINS PROPRIETARY INFORMATION

Figure 5.8.3 - Scenario 2b Full Core Offload with 105 deg. F CCW
Net Heat Load, Passive Heat Loss and Bulk Temperature Profiles



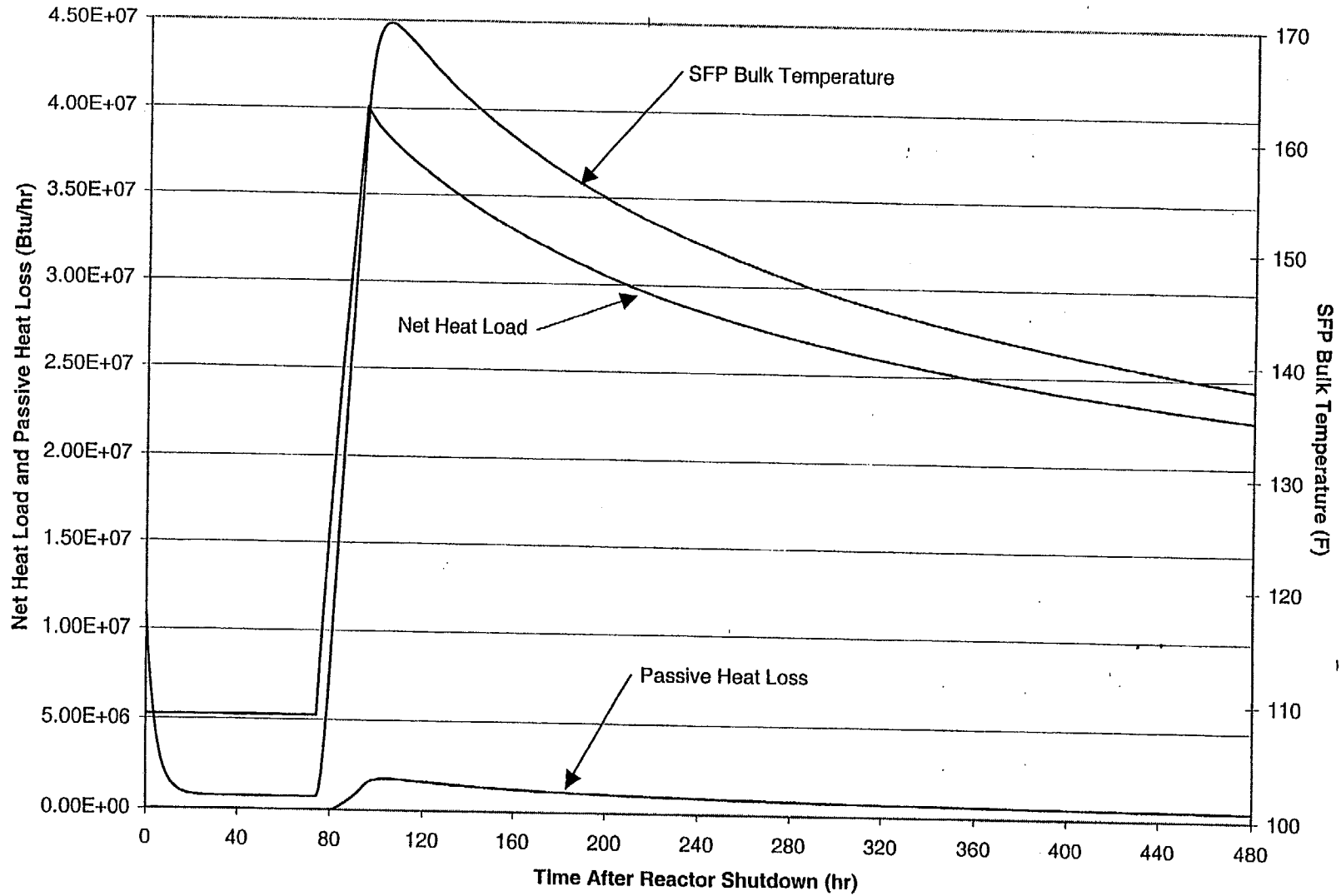
SHADED TEXT CONTAINS PROPRIETARY INFORMATION

Figure 5.8.4 - Scenario 2b Full Core Offload with 95 deg. F CCW
Net Heat Load, Passive Heat Loss and Bulk Temperature Profiles



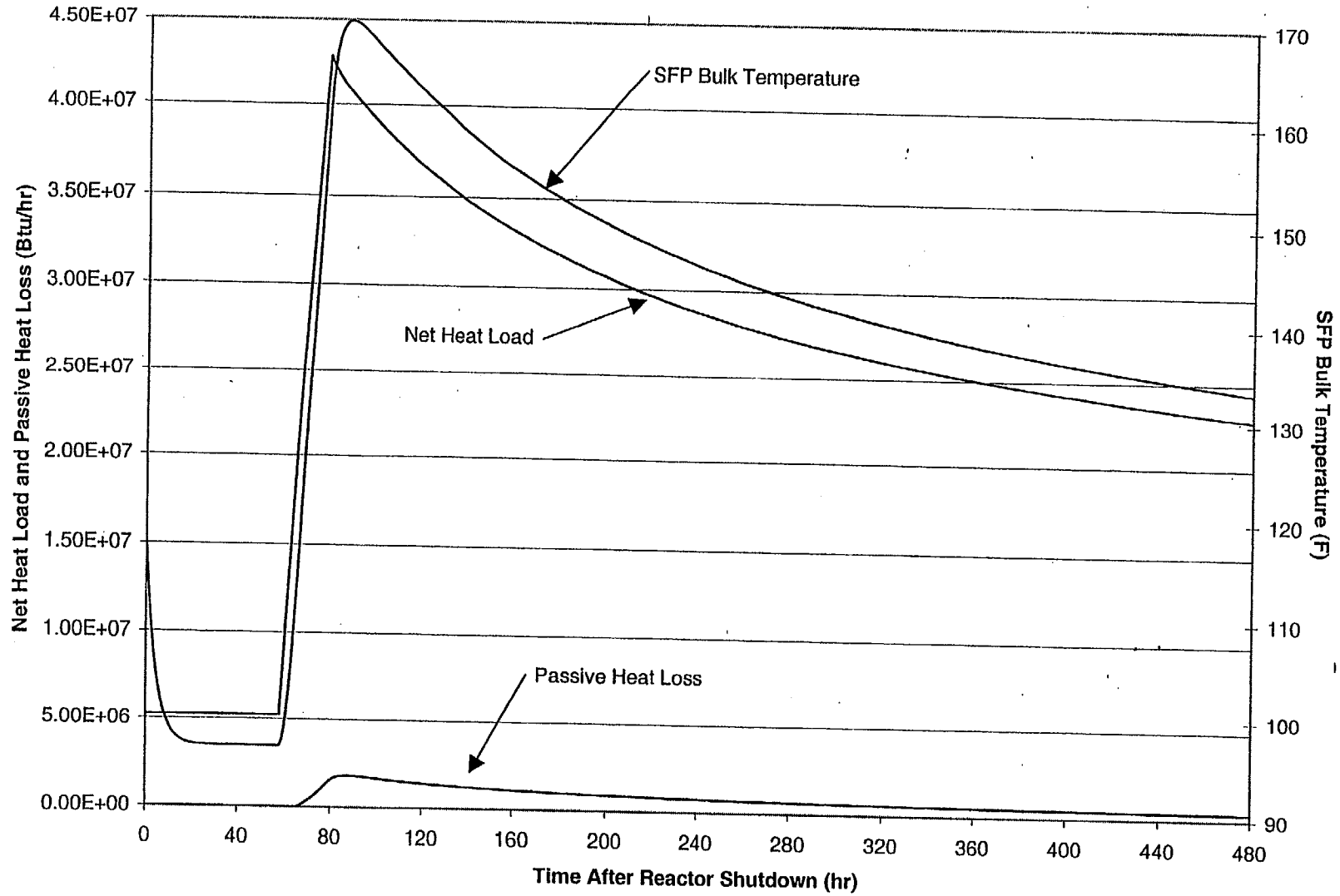
SHADED TEXT CONTAINS PROPRIETARY INFORMATION

Figure 5.8.5 - Scenario 2b Full Core Offload with 90 deg. F CCW
Net Heat Load, Passive Heat Loss and Bulk Temperature Profiles



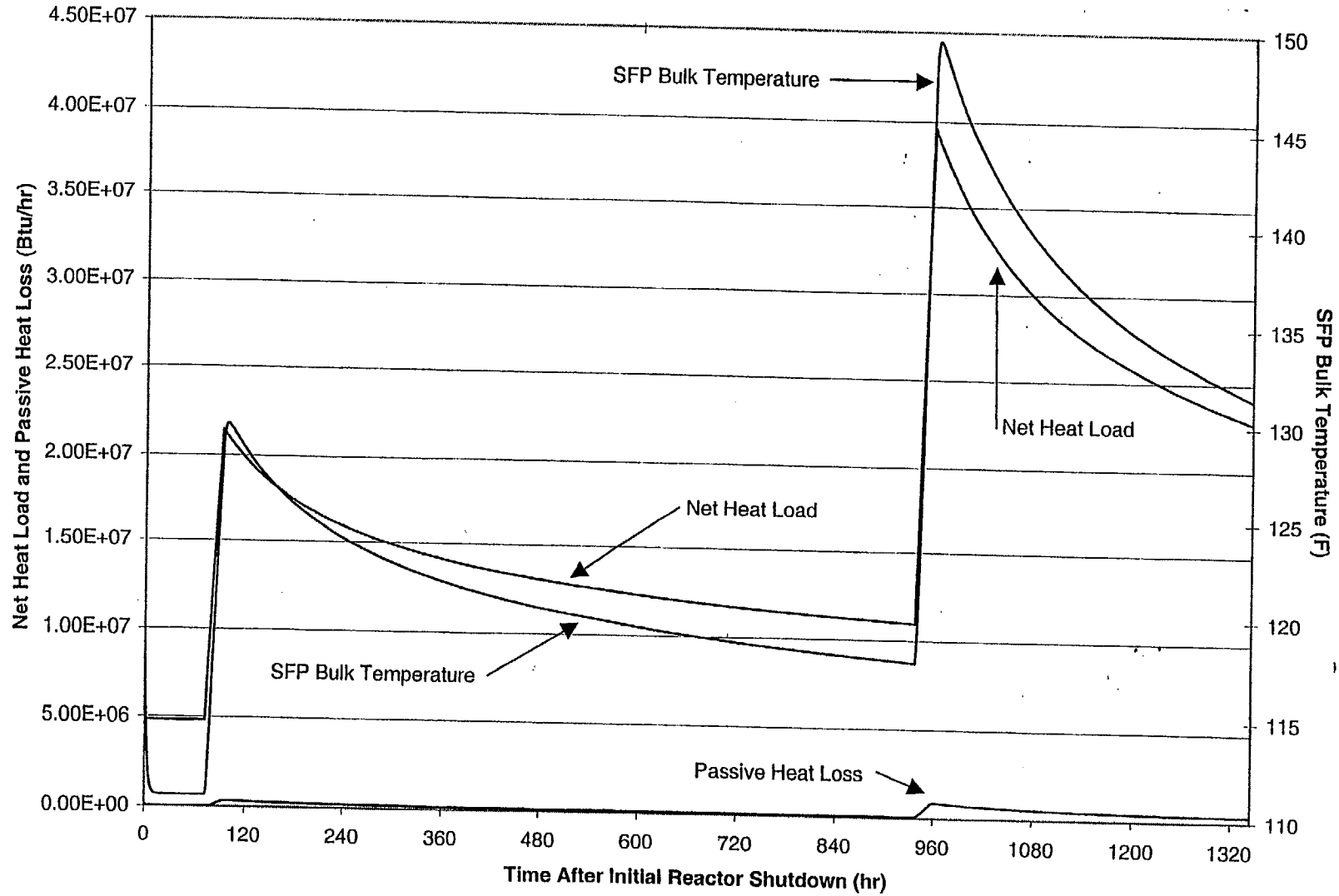
SHADED TEXT CONTAINS PROPRIETARY INFORMATION

Figure 5.8.6 - Scenario 2b Full Core Offload with 85 deg. F CCW
Net Heat Load, Passive Heat Loss and Bulk Temperature Profiles



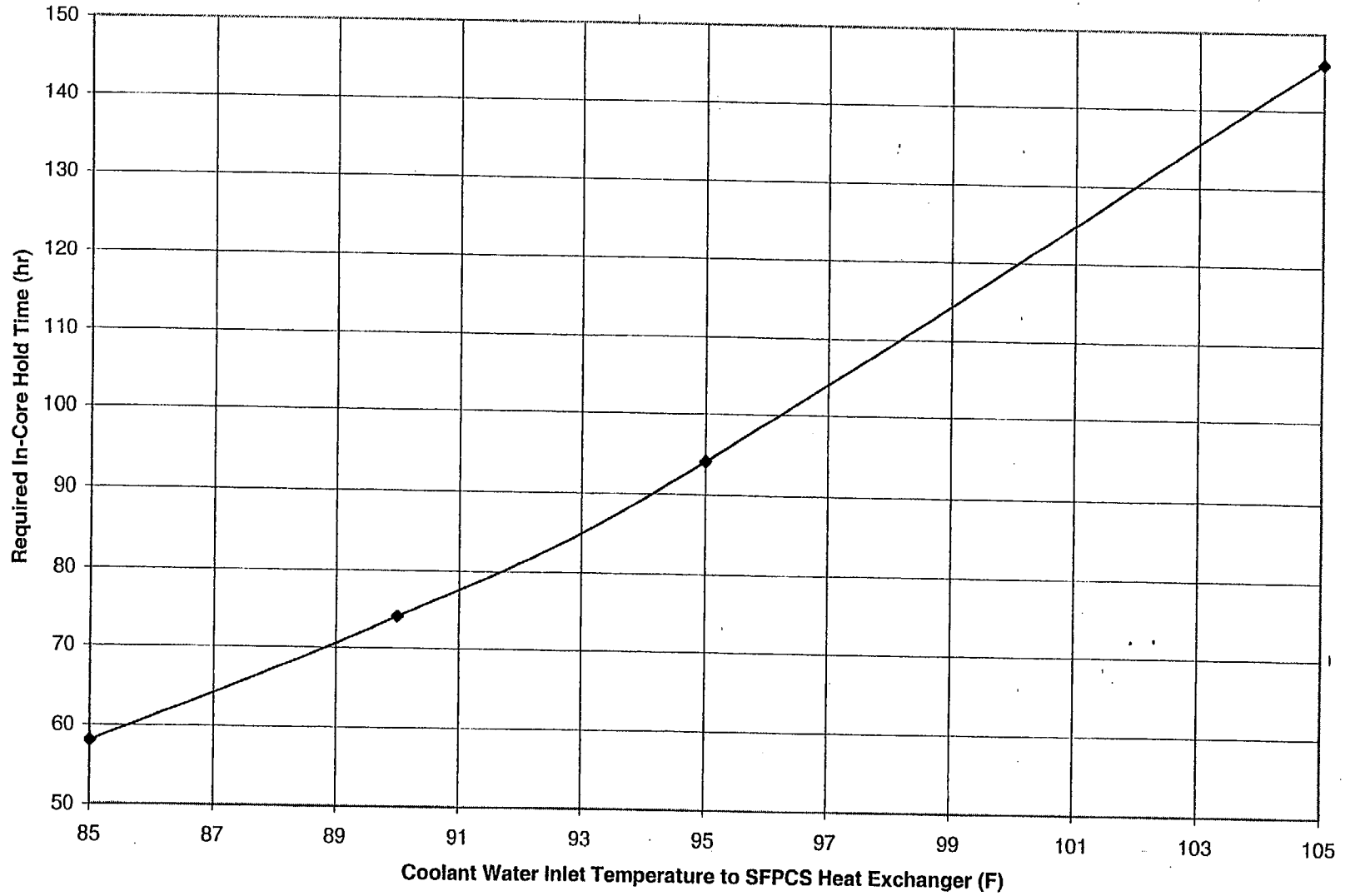
SHADED TEXT CONTAINS PROPRIETARY INFORMATION

Figure 5.8.7 - Scenario 3 Abnormal Full Core Offload
Net Heat Load, Passive Heat Loss and Bulk Temperature Profiles



SHADED TEXT CONTAINS PROPRIETARY INFORMATION

Figure 5.8.8 - Required In-Core Hold Time vs. Coolant Water Temperature
Scenario 2b Full Core Offload with One Cooling Loop Scenarios

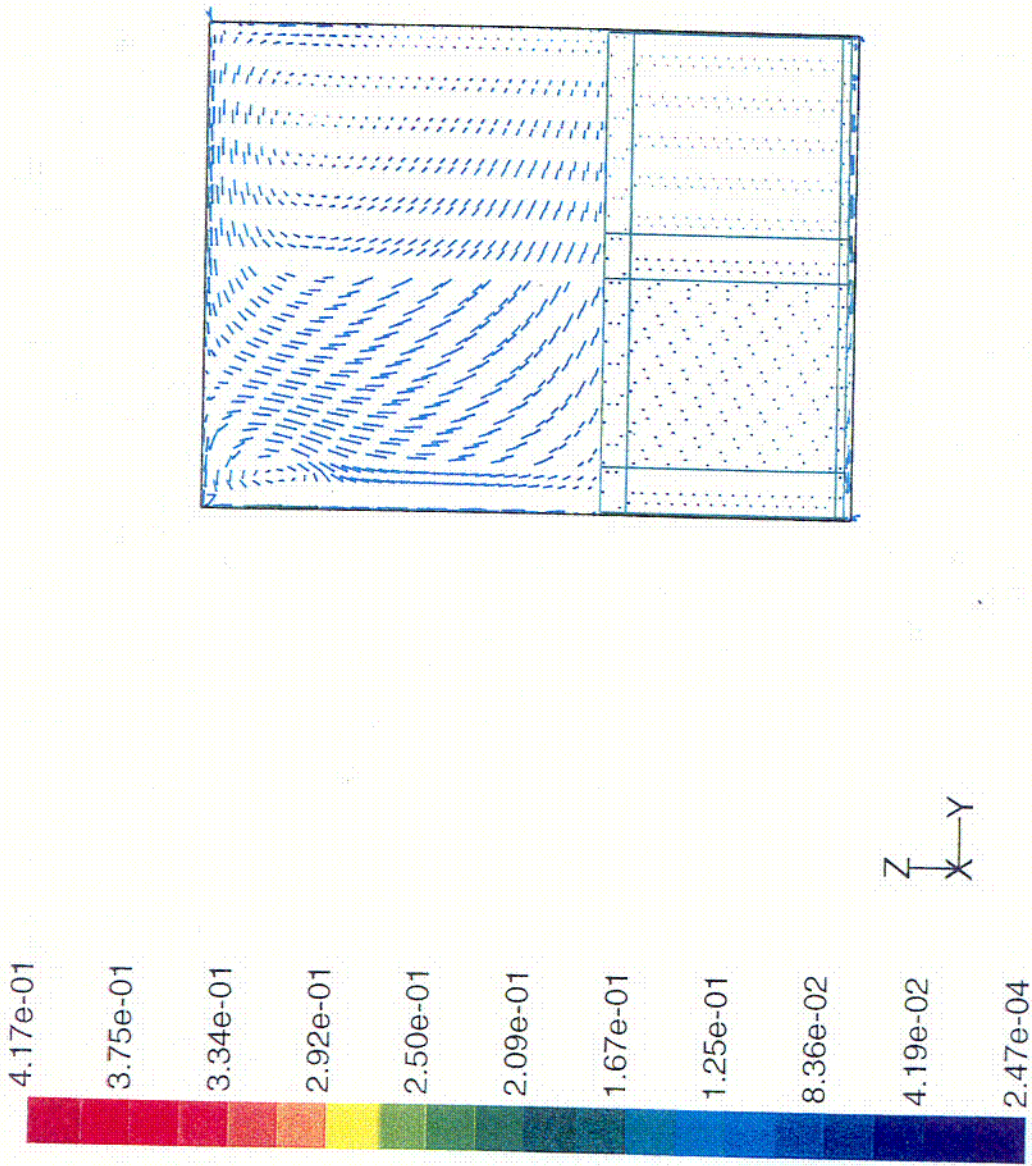




Contours of Static Temperature (k)

Apr 12, 2001
FLUENT 5.1 (3d, segregated, ke)

Figure 5.8.9 - Converged Temperature Contours from the Three-Dimensional CFD Model of the V.C. Summer SFP



Velocity Vectors Colored By Velocity Magnitude (m/s)

Apr 12, 2001
FLUENT 5.1 (3d, segregated, ke)

Figure 5.8.10 - Converged Velocity Vectors from the Three-Dimensional CFD Model of the V.C. Summer SFP